BAW-1286
Ca-7

RESONANCE ABSORPTION IN THORIUM METAL AND OXIDE RODS

JOINT U.S.-EURATOM RESEARCH AND DEVELOPMENT PROGRAM

Final Report

November, 1963

By
W. G. Pettus
M. N. Baldwin
Critical Experiment Laboratory

C. Samuel
EURATOM Representative

Submitted to
THE UNITED STATES ATOMIC ENERGY COMMISSION
By
THE BABCOCK & WILCOX COMPANY
Nuclear Development Center
Lynchburg, Virginia

DISCLAIMER

FOREWORD

The United States and the European Atomic Energy Community (EURATOM), on May 29 and June 18, 1958, signed an agreement which provides a basis for cooperation in programs for the advancement of the peaceful applications of atomic energy. This agreement, in part, provides for the establishment of a Joint U. S. - Euratom research and development program which is aimed at reactors to be constructed in Europe under the Joint Program.

The work described in this report represents the Joint U. S. - Euratom effort which is in keeping with the spirit of cooperation in contributing to the common good by the sharing of scientific and technical information and minimizing the duplication of effort by the limited pool of technical talent available in Western Europe and the United States.

ACKNOWLEDGMENTS

The authors are indebted to Mr. R. H. Lewis, Mr. J. W. Poston, and Mr. J. F. Carson for assistance in the experimental operations, and to Mr. W. A. Wittkopf and Mr. R. J. Neuhold for assistance in the analysis.

ABSTRACT

Measurements of the resonance capture integral and associated phenomena for Th and ThO_2 rods have been made using primarily an activation technique. The effective resonance integral (above 1/v) at room temperature is given by

$$I_{Th} = 3.91 + 14.81 \sqrt{S/M} \quad \text{barns}$$

$$I_{ThO_2} = 3.41 + 17.32 \sqrt{S/M} \quad \text{barns}$$

for rods from 0.4 to 2.9 cm diameter. The temperature dependence for a 0.68 cm rod is given by

$$I(T) = I(T_o)\left[1 + 0.016\left(\sqrt{T} - \sqrt{T_o}\right)\right]$$

where T is the Kelvin absolute temperature. The treatment of Dancoff and Ginsburg to account for the mutual shielding of parallel rods is confirmed by direct measurement.

CONTENTS

CONTENTS (Cont'd)

List of Tables

List of Figures

1. INTRODUCTION

1.1. Preliminary Information

The experiments reported here constitute an investigation of neutron resonance capture integrals for thorium under various conditions. The effects of rod size, temperature, and shadowing by neighboring rods have been measured using primarily the activation technique. Similar measurements have previously been made at this Laboratory in the same experimental facility by the reactivity method. The use of a different and independent measurement technique in the present work is intended to expose any systematic errors which may be introduced by the apparatus or experimental procedure associated with either of the two methods.

Apparently no comparable work using both techniques at the same facility has been reported. There have been a number of previous measurements, yielding rather widely different results, by one or the other method. Both methods have, however, been previously used at this Laboratory for Uranium-238 resonance integral measurements and the results were in agreement within the uncertainties in the calibration standards. These measurements are described in detail in BAW-1244.

1.2. Outline of Scope and Objectives

The primary objectives of the present work were as follows:

1. the determination of the variation of the effective resonance integrals of thorium and thorium oxide rods with rod diameter over the range of practical interest
2. the determination of the variation of the effective resonance integral of a thorium oxide rod with temperature from room temperature to 800°C

3. the determination of the reduction of the effective resonance integral (Dancoff effect) of an absorbing rod caused by a parallel neighboring rod of the same material.

For the diameter dependence measurements the sample diameters were in the range from 1/4 inch to 1 1/4 inch for both thorium metal and oxide. Both the metal and oxide samples were approximately 6 inches in length. The metal rods consisted of machined cylinders while the oxide rods consisted of stacks of sintered pellets.

In the temperature dependence measurements the test rod diameter was 0.266 in. in diameter and 6 in. long. Relative activation measurements were made at room temperature, 200, 500, and 800°C.

For the Dancoff measurements the rod diameter was approximately 3/8 in. for both thorium oxide and uranium oxide. The moderating medium between the rods was D_2O and the center-to-center spacing varied from 0.442 in. to 1.037 in.

1.3. Methods of Measurement

The primary facility for all measurements reported here was the Lynchburg Pool Reactor (LPR). In each case the samples were cadmium shielded and located at the center of the core. For the diameter dependence measurements both the activation and the reactivity methods were used. In the activation case a test sample from the center of the rod was dissolved and the separated Pa^{233} was gamma counted. These measurements were calibrated with reference to the infinitely dilute resonance integral of Th^{232}. In the reactivity case the reactivity coefficients were deduced from period measurements and the calibration was with reference to infinitely dilute boron.

For the temperature dependence measurements the samples were uniformly heated and held at constant temperature during the activation. The subsequent chemical and counting procedures were the same as in the geometric dependence investigation.

For the Dancoff measurements the activation technique was used in all cases. The rod containing the counting sample was cadmium clad and the shielding rod was aluminum clad. The same test

assembly was used in both the ThO_2 and the UO_2 cases. In the UO_2 cases the Np^{239} activity was used as a measure of the neutron capture in the resonance region.

THIS PAGE
WAS INTENTIONALLY
LEFT BLANK

2. EXPERIMENTAL FACILITIES AND APPARATUS

2.1. Lynchburg Pool Reactor

All experimental measurements in the present investigation were carried out at the Lynchburg Pool Reactor (LPR). (See Figs. 2-1, 2-2, and 2-3.) The measurements were made with the experimental sample at the center of the reactor approximately 17 feet below the pool surface. Fig. 2-4 shows the core configuration used in the geometric and temperature dependence measurements. Each MTR-type fuel element consists of 10 plates of uranium-aluminum alloy with about 19 grams of U^{235} in each plate. Each control element contains six plates of the same type. The central element position is occupied by a void test thimble which extends above the pool surface. The lower end of the thimble, which penetrates through the core, consists of a 1 5/8-inch OD cadmium tube with a 0.0226-inch wall sandwiched between two thin-walled aluminum tubes. An adjustable aluminum spacer is used at the bottom of the thimble to center the samples vertically in the core. The thimble is equipped with a plenum for forced cooling and a surface thermocouple for temperature monitoring.

Fig. 2-5 shows the core configuration used in the Dancoff effect measurements. In this case, the test thimble is a 3 by 3 inch square aluminum tube with no cadmium section. A test assembly consisting of a cadmium clad rod and an aluminum clad shielding rod in D_2O moderator is lowered to the center of the core through this thimble.

2.2. Sample Containment Assembly

The samples used in the geometric dependence measurement range in diameter from 0.158 to 1.155 inches. These samples are held in closely-fitting aluminum tubes, and a secondary container is used to center the samples in the test cavity within the reactor. The inner tube is secured in the outer tube by a screw-on cap which slips over the projected end fitting and rests on a shoulder of this fitting.

The holder assembly is shown in Fig. 2-6 with a typical sample of stacked ThO_2 pellets. Pellet alignment is maintained by the close-fitting cladding tube. This tube is centered by a mechanical constraint in the outer holder, which is coupled by a short rod to a light chain for insertion and withdrawal of the assembly. All components of the holder assembly are made of aluminum except a small stainless-steel set screw in the coupling rod.

2.3. Sample Heaters and Temperature Measurement System

The thorium-oxide sample for the Doppler coefficient measurements consisted of stacked pellets, half of which contained a 0.050-inch hole for axial placement of a thermocouple. The pellets were contained in a stainless steel tube insulated with mica and wound with a nichrome heater as shown in Fig. 2-7. The heater was closely wrapped with asbestos paper, and the assembly was centered in a polished stainless steel container with Kaowool insulation between the heater assembly and the walls of the container. A second thermocouple was inserted along the can wall to monitor temperature near the inside of the cadmium thimble, which enclosed the assembly shown in Fig. 2-7. A third thermocouple was secured to the outside of the thimble to measure the water temperature.

2.4. Dancoff Test Assembly

The sample container for the Dancoff measurements was a thin-walled aluminum extrusion, 2.814 inches square in cross section, with a welded bottom and a detachable top. This container is fitted with celluloid top and bottom spacing plates and an 18 mil wall by 0.412-inch OD cadmium jacket for the central rod. The parallel shielding rod is aluminum clad and is clamped in position on the spacing plates by stainless steel screws. The components of this assembly are shown in Fig. 2-8.

2.5. Chemical Processing Facilities

Dissolving the thorium oxide sample pellets requires prolonged (one to three weeks) boiling in aqua regia. This is done in refluxing units as shown in Fig. 2-9. An ion-exchange process is used to separate the Pa^{233} from the solution and the resin column used for this separation is shown in Fig. 2-10.

2.6. Counting Equipment

The separated sample solutions are gamma-counted on a 3 inch sodium-iodide crystal as shown in Fig. 2-11. The lucite ring over the crystal is used to center the flasks containing the counting solutions. The crystal unit is located at the center of a copper lined 4 foot cubical lead cave with 4 inch thick walls and top. The pulse height analysis is done with the 400 channel analyzer system shown in Fig. 2-12.

The gold monitor foils are beta-counted in shielded methane-flow proportional counters (Fig. 2-13) in conjunction with the standard amplifiers and scalers.

2.7. Data Reduction Facilities

Machine computation was employed wherever it was feasible with most of the work being done on the Burroughs 205 and Philco 211. The IBM 7090 was also used briefly for an AIM-6 calculation of certain properties of the LPR core.

Fig. 2-1. LPR Core for Geometric and Temperature Dependence Measurements

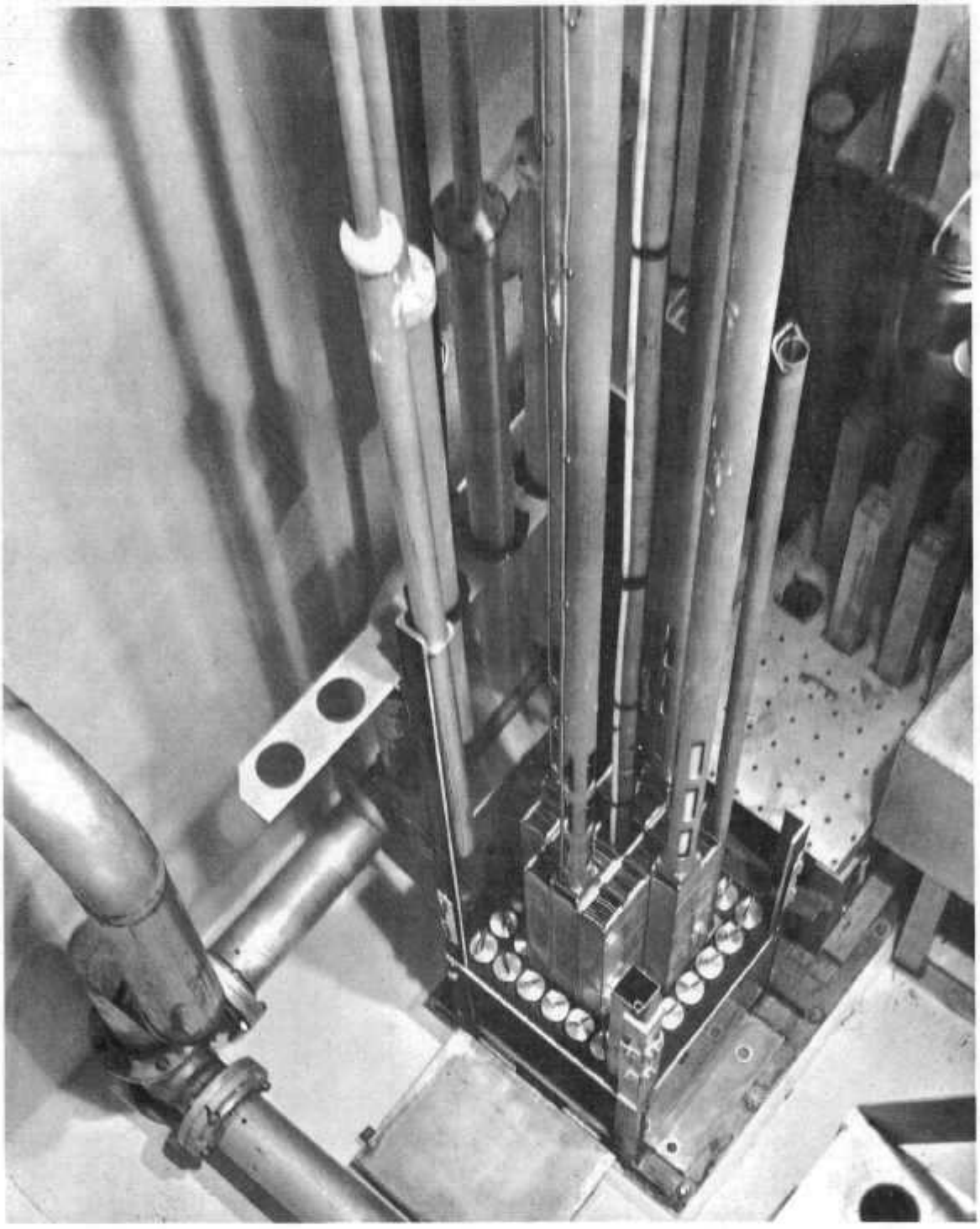

Fig. 2-2. LPR Core for Dancoff Effect Measurements

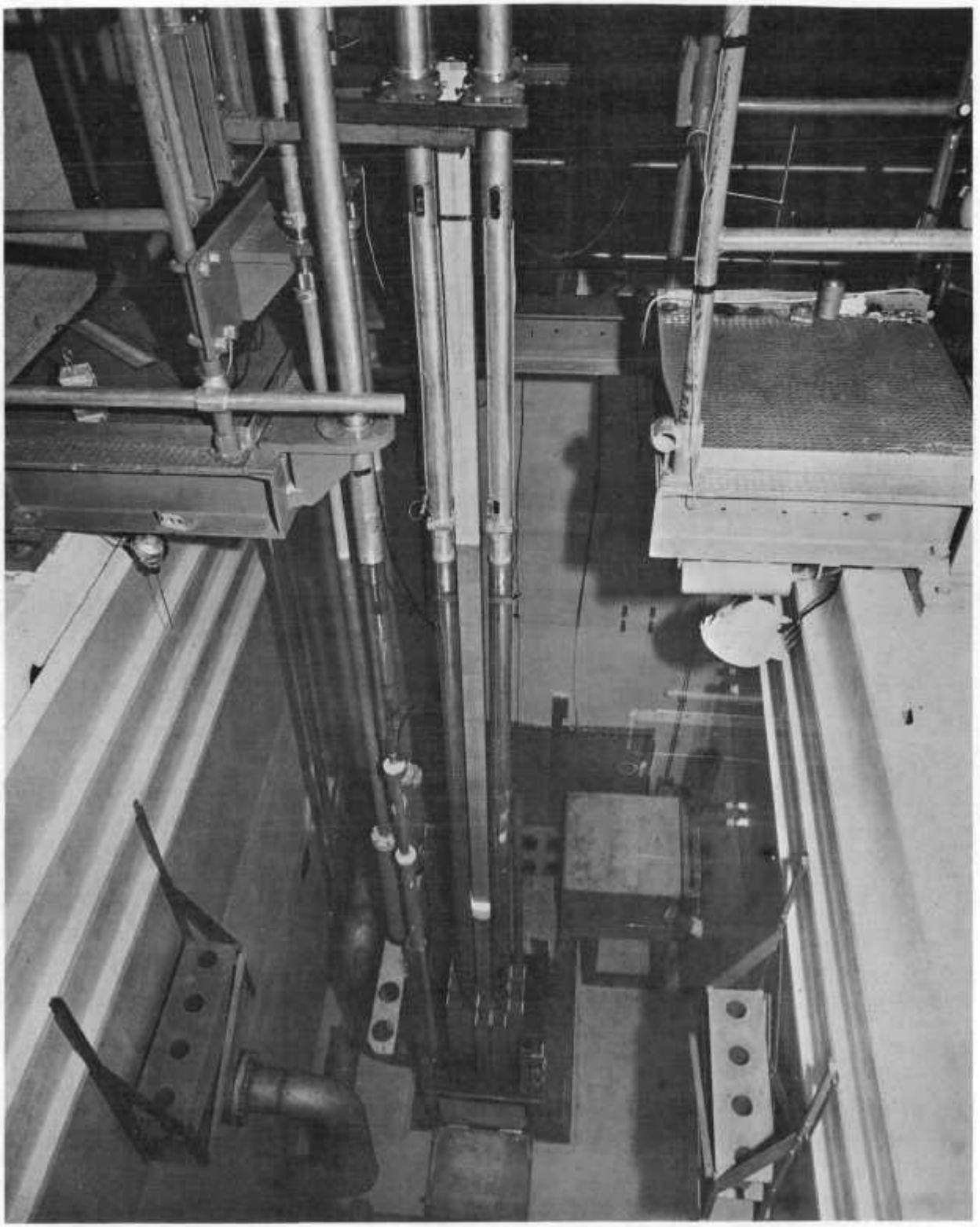

Fig. 2-3. LPR Instrumentation

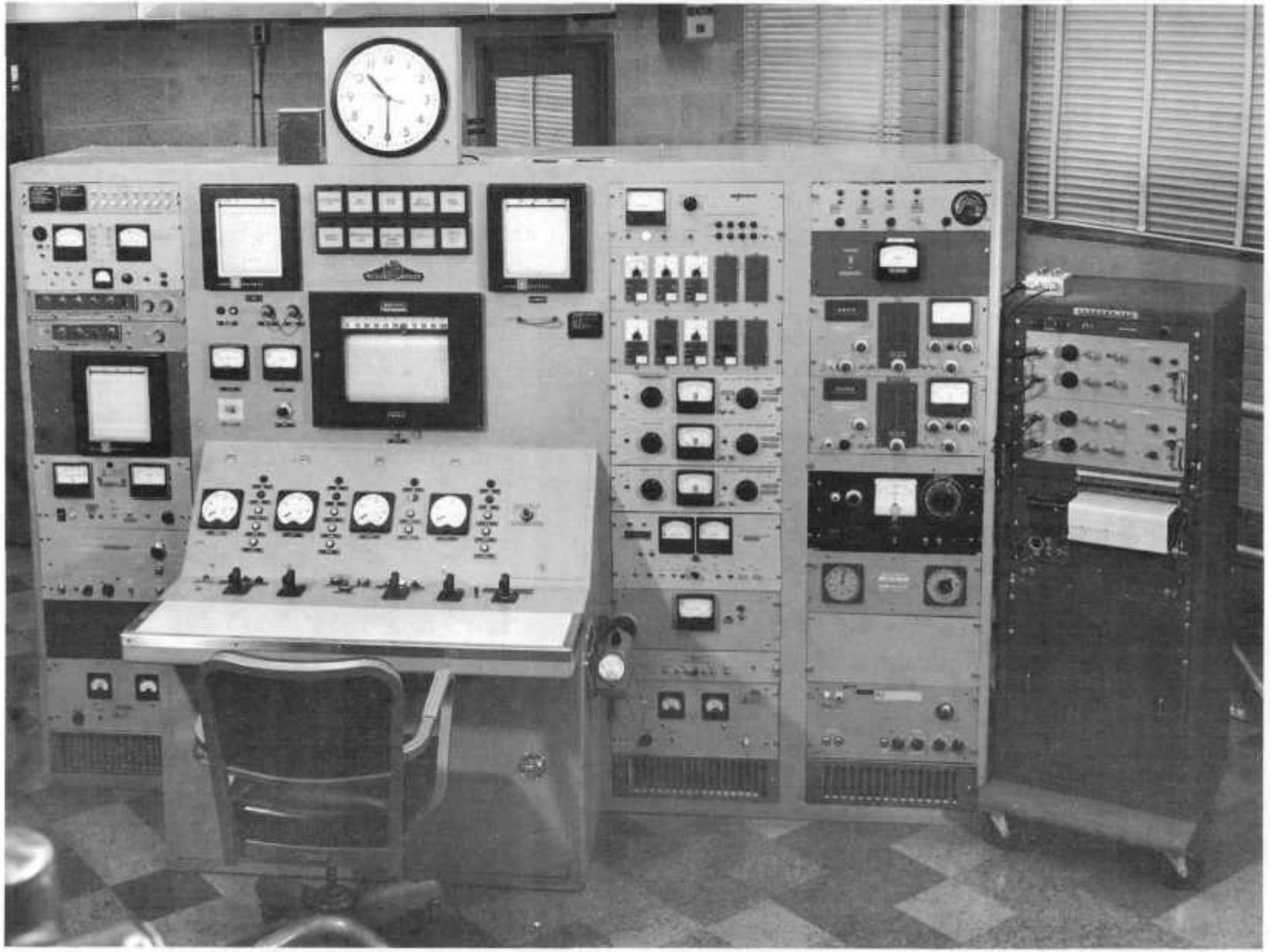

Fig. 2-4. Core Configuration for Geometric and Temperature Dependence Measurements

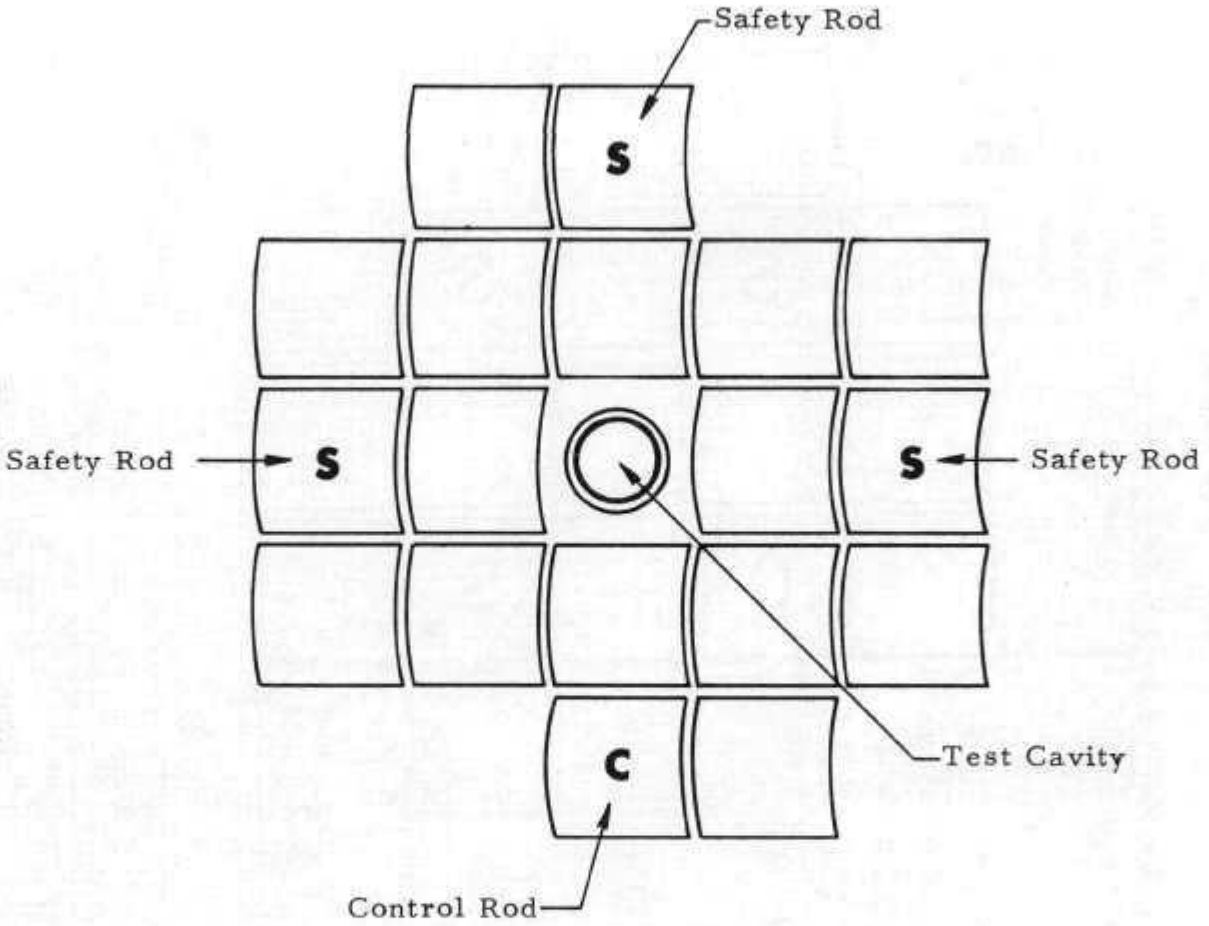

Fig. 2-5. Core Configuration used in the Dancoff Measurements

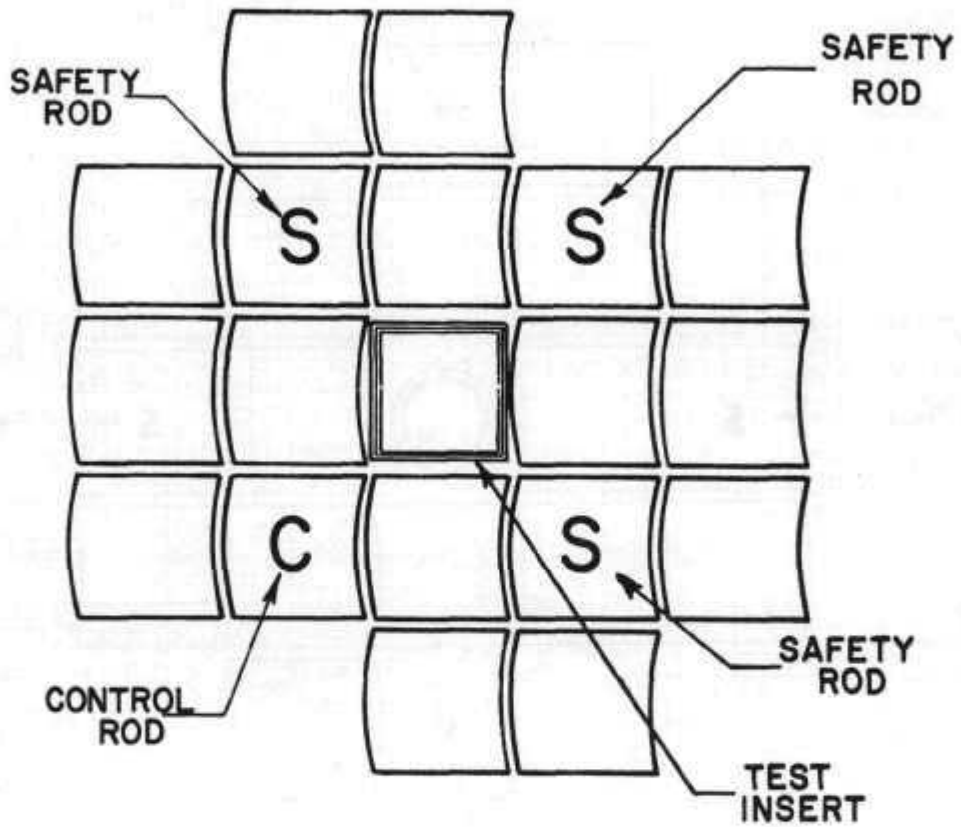

Fig. 2-6. Sample Holder Assembly

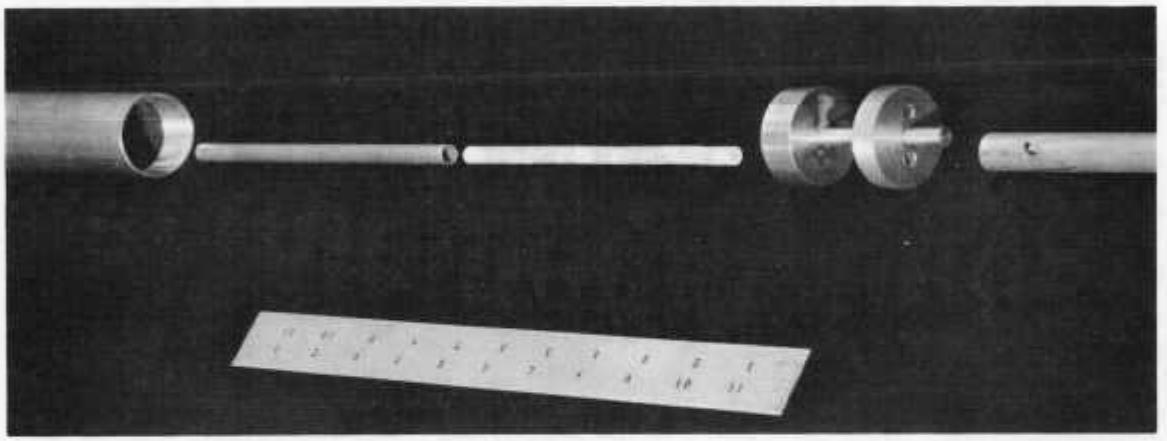

Fig. 2-7. Heated Sample Assembly

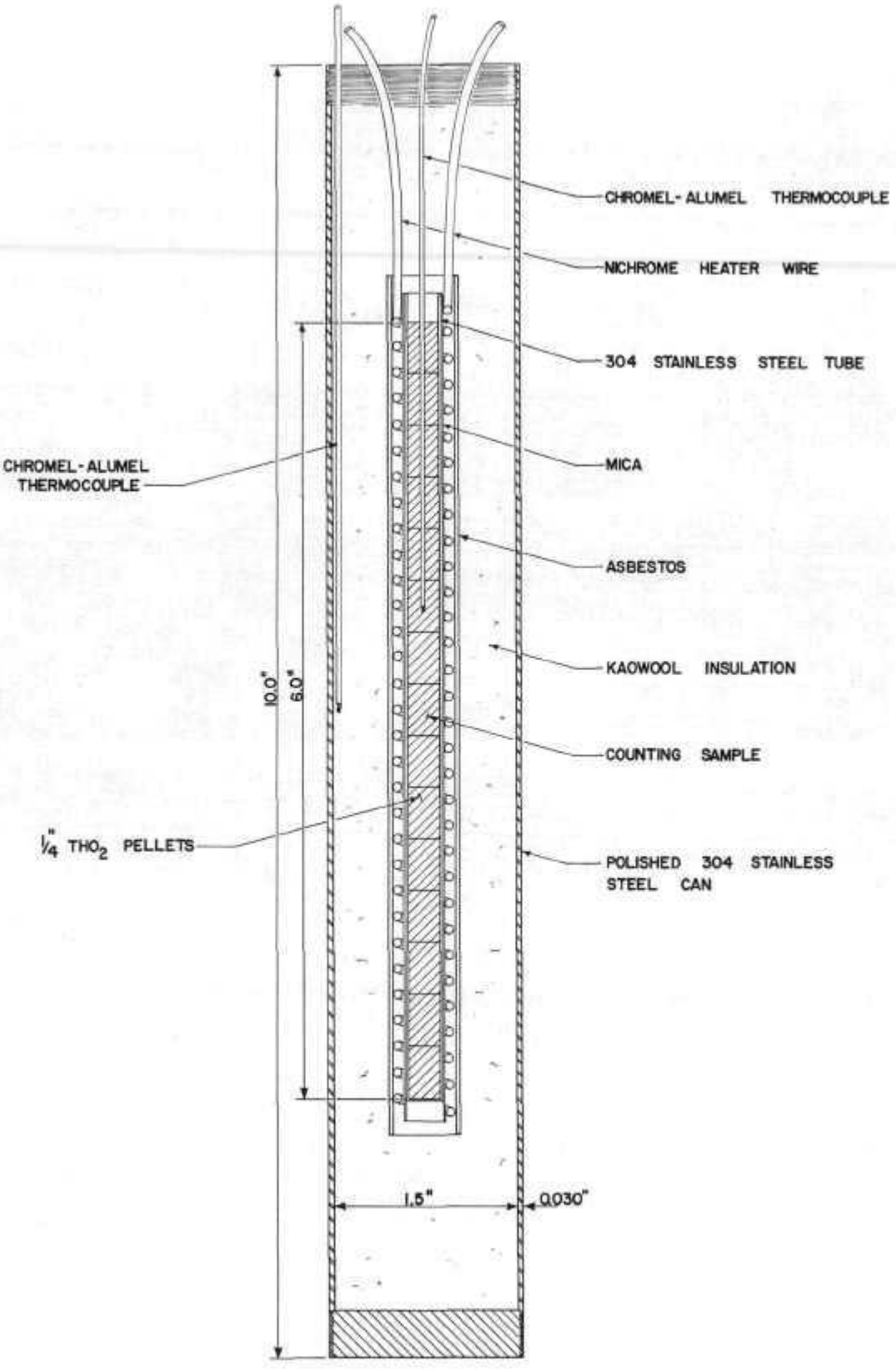

Fig. 2-8. Dancoff Measurement Assembly

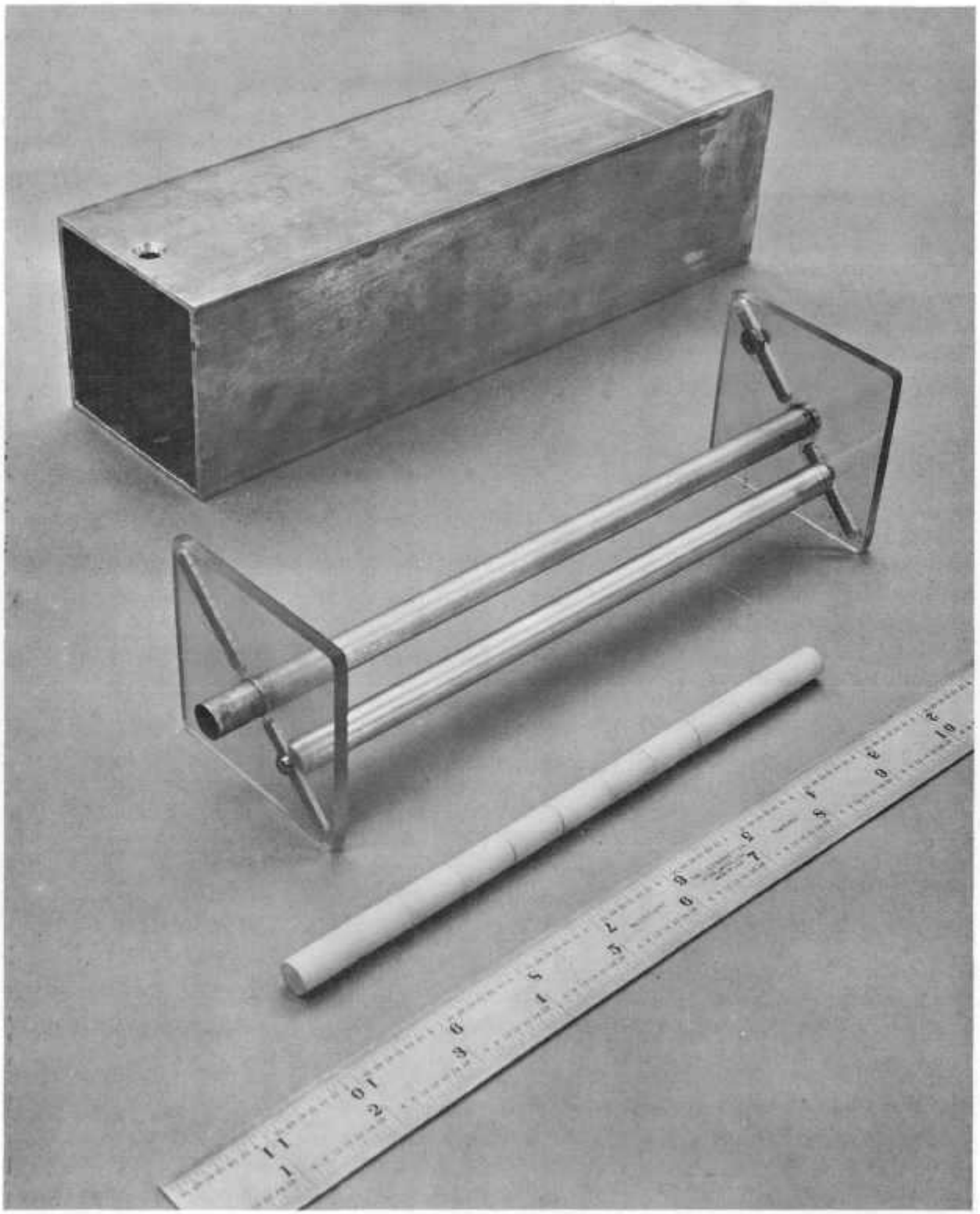

Fig. 2-9. Refluxing Apparatus

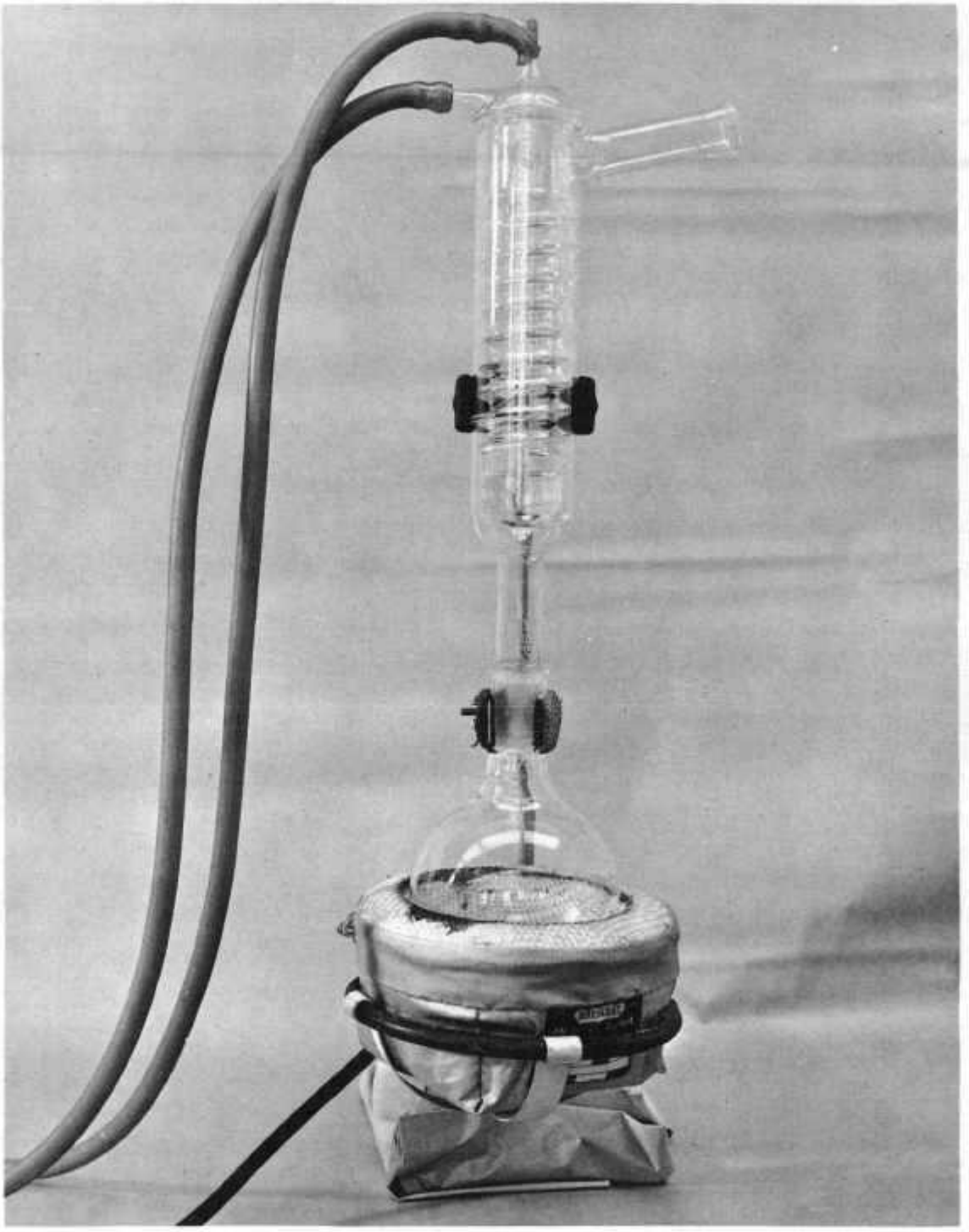

Fig. 2-10. Resin Column

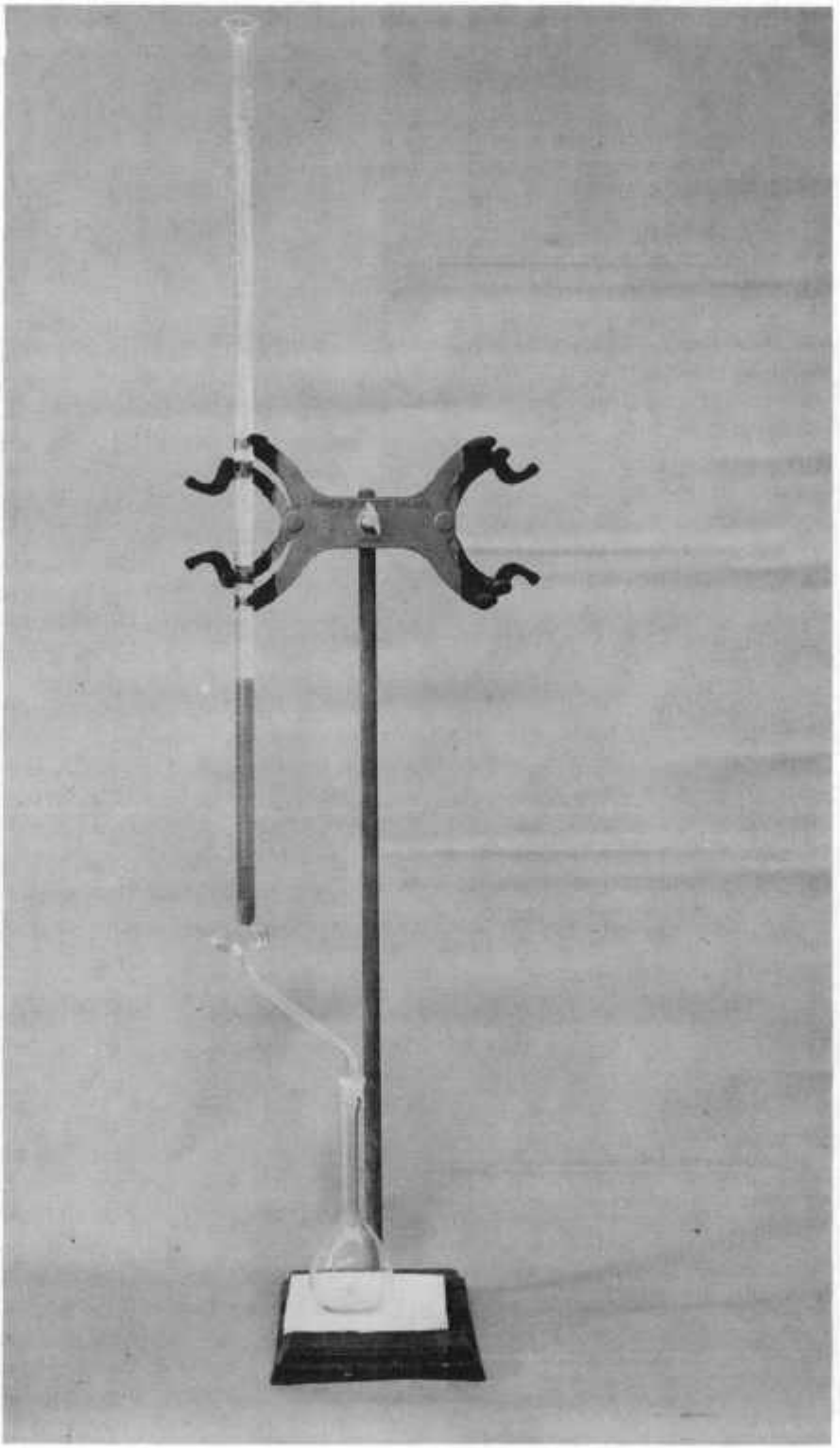

Fig. 2-11. Detector Crystal and Sample Solution

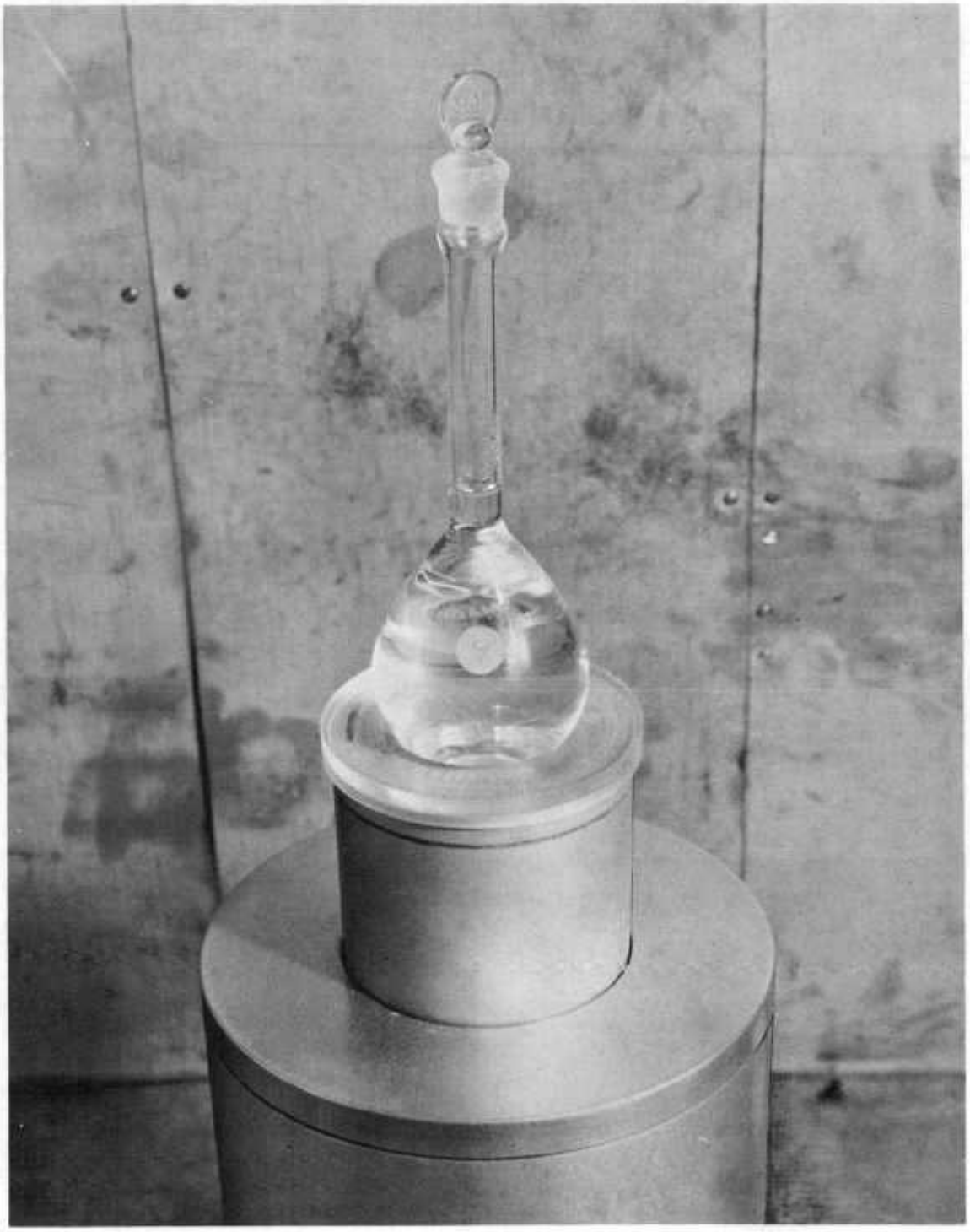

Fig. 2-12. 400-Channel Analyzer and Data-Readout System

Fig. 2-13. Proportional Counter

3. LPR CHARACTERISTICS

3.1. Information Required for Data Interpretation

In order to compare measured resonance integrals with the highly idealized theoretical calculations it is necessary to account for the departure of the experimental conditions from those assumed in the calculations. This requires a knowledge of the neutron spectrum at the sample position inside the cadmium tube. In addition the intercomparison of reactivity measurements requires a knowledge of the neutron importance spectrum and the spatial flux shape. The determination of these properties is described below.

3.2. Neutron Spectrum

The most detailed picture of the neutron spectrum in the cadmium tube has been obtained from a 5 region, 75 group, cylindrical P1MG calculation. This spectrum is shown in Fig. 3-1 and agrees very well with an earlier multigroup diffusion calculation previously reported.[1] Here the zero of lethargy is taken as 10 mev. The spectrum is essentially 1/E over the resolved resonance region but rises somewhat in the fission region and drops sharply near the cadmium cutoff.

3.3. Importance Spectrum

The cadmium sleeve has a severe effect on the importance function as well as on the neutron spectrum near and below the cadmium cutoff. This is due to the fact that some neutrons which are captured in the sample would have been captured in the cadmium sleeve anyway and therefore are not detected in a reactivity measurement. In the region near the cadmium cutoff where these events are highly probable the importance drops sharply to zero. Also the importance drops slightly at high energy due to the increase in the reactor escape probability. Since the P1MG code does not compute group

adjoints the relative importance for each group has been obtained from a smooth curve drawn through calculated points from 18 group AIM-6 adjoint calculations. The results are shown in Fig. 3-2.

3.4. Flux Shape in the Test Cavity

A set of gold foils mounted on an aluminum bar was used to measure the epicadmium flux distribution along the axis of the cadmium thimble. Each foil (1/4 inch in diameter and 0.005 inch thick) was held in a small aluminum cover. The result of this traverse is shown in Fig. 3-3. The occurrence of the flux maximum at the vertical center of the core verifies that the sample activations are carried out in essentially a zero-gradient position. This condition is a consequence of the core loading, in which the rods are well removed from the test thimble, the three shims are fully withdrawn, and the regulating rod is almost fully withdrawn.

Fig. 3-1. Relative Flux Spectrum in the LPR Cadmium Thimble

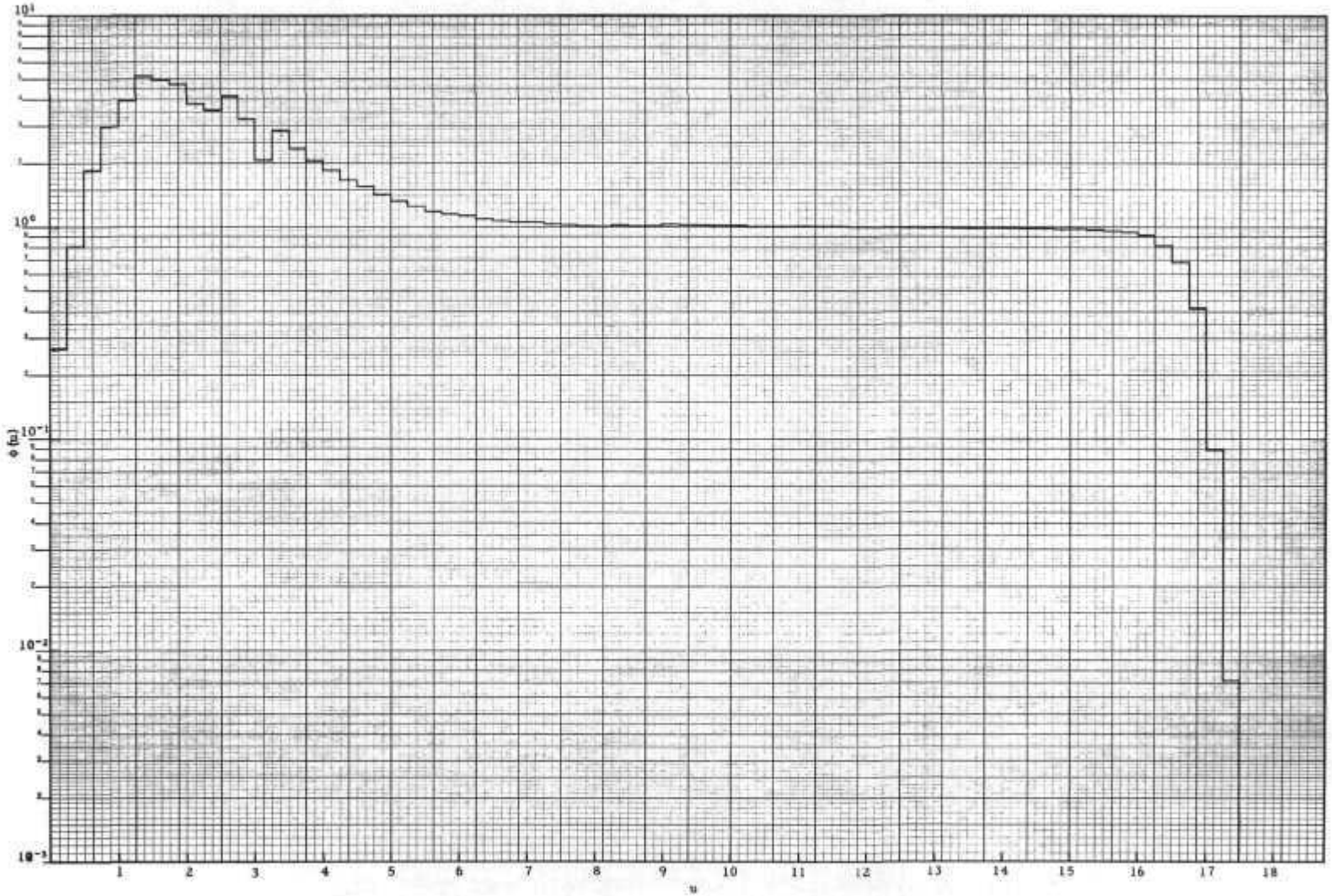

Fig. 3-2. Relative Importance Spectrum in the LPR Cadmium Thimble

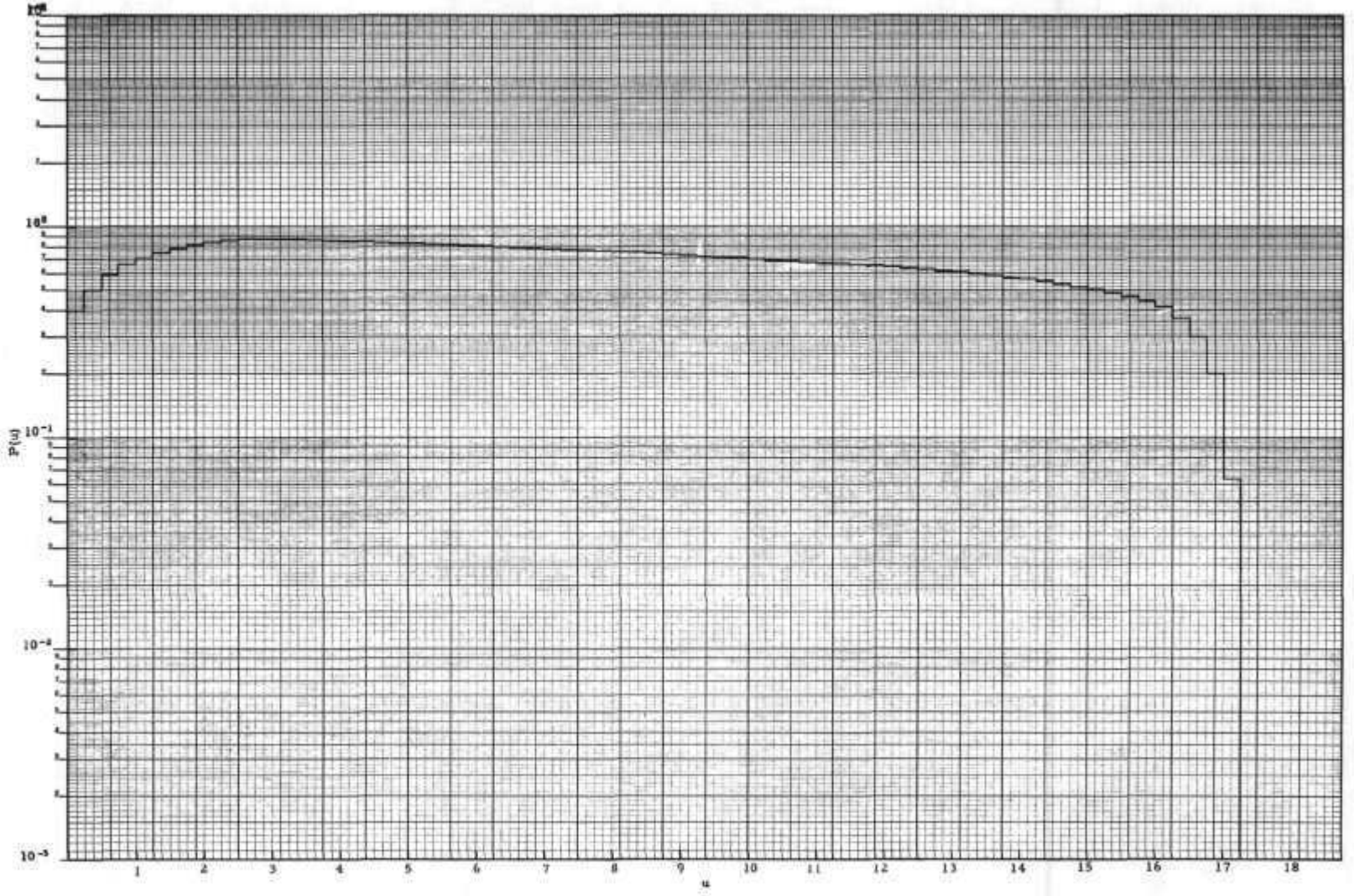

Fig. 3-3. Vertical Flux Distribution in LPR Cadmium Thimble

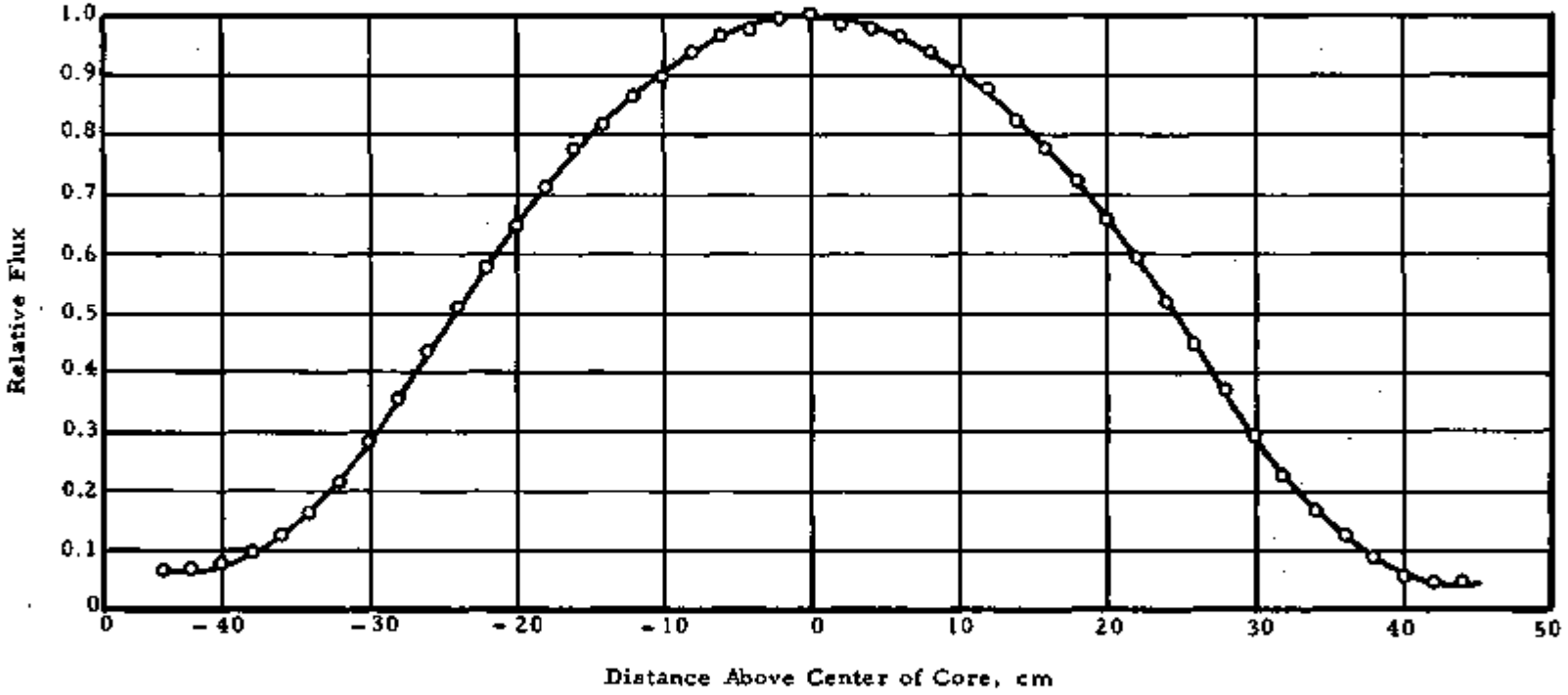

THIS PAGE
WAS INTENTIONALLY
LEFT BLANK

4. EXPERIMENTAL SAMPLES

4.1. Samples for Geometric Dependence Measurements

The thorium metal samples used in these measurements were made up of two 3 inch long rods of circular cross-section. The rods were machined to a smooth finish with accurately matching end faces. The oxide samples consisted of stacks of sintered pellets held in accurate alignment by close-fitting aluminum tubes. Table 4-1 gives the parameters of these samples.

For the activation measurements, small disks or pellets as shown in Fig. 4-1 were placed at the vertical center of the bulk sample. These counting samples were of the same material and of precisely the same diameter as the bulk samples and were held in accurate alignment by the aluminum cladding.

4.2. Samples for Doppler Coefficient Measurements

The Doppler coefficient measurements were made with a 6 in. long by 0.266 inch diameter thorium oxide rod having a density of 9.12 gm/cm^3. The center pellet of the stack was replaced with an unirradiated pellet for each run and the irradiated pellet was dissolved and used as the counting sample. A chromel-alumel thermocouple was inserted through a 50 mil axial hole in the upper pellets and embedded in the second pellet above the counting sample as shown in Fig. 2-7.

4.3. Samples for Dancoff Effect Measurements

The Dancoff measurements were made using both thorium oxide and depleted (approximately 350 ppm U^{235}) uranium oxide rods of approximately the same size. The exact thorium oxide rod diameter was 0.364 in. and that for the uranium oxide was 0.358 in. In each case the rod length was approximately 7.5 in. The average

density of the thorium oxide rods was 9.39 gm/cm^3 and that for the uranium oxide was 10.24 gm/cm^3 . The central rod and the shielding rod were essentially identical in each case. The center pellet of the central rod was used as the counting sample and this was replaced with an unirradiated pellet before each run.

4.4. Activity Calibration Samples

The activation measurements were calibrated with respect to the infinite dilution resonance integral of thorium. This required a measurement of the ratio of the specific activity of an irradiated rod sample to that of an extremely thin film. The thin samples were made by depositing 0.20 mg of thorium from a thorium solution on to Teflon planchets and allowing them to dry uniformly over an area of about 1 cm^2 . The rod samples were obtained by dissolving the irradiated thorium disks described in Section 4.1 and depositing 0.20 mg on identical Teflon planchets. This procedure provided identical counting geometry for the subsequent β-counting.

4.5. Reactivity Calibration Samples

The calibration samples for the reactivity measurements consisted of four dilute dispersions of elemental boron powder (325 mesh) in aluminum powder held in six-inch-long aluminum tubes, 0.25 inches in OD and 0.035 inches in wall thickness. The amount of boron contained in these samples varied from 0.059 to 0.301 grams. Other samples with identical dimensions but no boron in one case and neither boron nor aluminum powder in another case were provided for reference measurements.

4.6. Miscellaneous Samples

Reactivity measurements were made on samples of aluminum, aluminum oxide, and bismuth to determine the necessary corrections for scattering in thorium and thorium oxide.

Table 4-1. Sample Parameters

Material	Diameter, cm	Length, cm	Mass, gm	Density, gm/cm^3	$\sqrt{S/M}$ (cm $gm^{-1/2}$) Excluding Ends	$\sqrt{S/M}$ (cm $gm^{-1/2}$) Including Ends
Th	0.401	14.78	21.72	11.62	0.926	0.933
Th	1.008	14.91	138.37	11.62	0.584	0.594
Th	2.934	14.61	1148.00	11.62	0.342	0.359
ThO_2	0.401	14.40	13.09	7.19	1.178	1.186
ThO_2	0.676	14.83	48.50	9.12	0.806	0.815
ThO_2	2.377	11.40	359.39	7.10	0.487	0.511
ThO_2	2.934	14.29	690.68	7.15	0.437	0.459

Fig. 4-1. Typical Counting Samples of Thorium Metal and Oxide

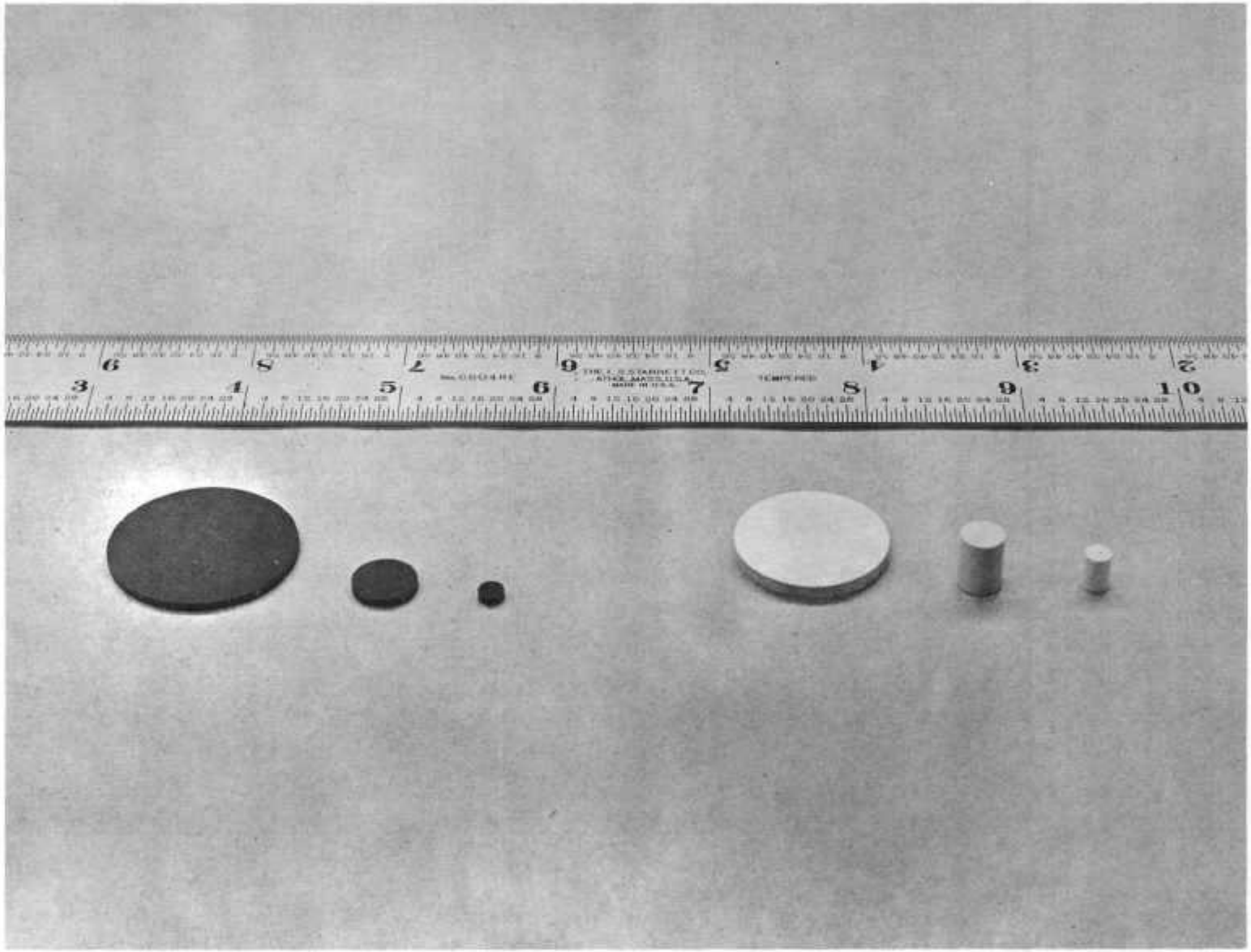

5. EXPERIMENTAL PROCEDURES

5.1. Sample Activation

The activation samples, held in a container assembly as shown in Fig. 2-6, were lowered through the void access thimble to the center of the LPR core where they rested on a stationary aluminum plug. Ten minute exposures were made for all irradiations and the reactor power level was held at 0.5 to 10 kilowatts depending on the sample size. Each activation was monitored by a 0.25 in. diameter by 0.005 in. thick gold foil held in a water-tight aluminum container and located at an accurately reproducible position about 10 inches from the edge of the core.

5.2. Chemical Processing and Separation

In the present measurements the counting samples were of such varied sizes that direct counting was not feasible. The samples were therefore dissolved and counted in solution in volumetric flasks. In the process the protactinium was chemically separated from the thorium to minimize the background correction.

The Th^{233} formed in the (n, γ) reaction in Th^{232} decays by the following scheme:

$$Th^{233} \xrightarrow[22.1\ m]{\beta} Pa^{233} \xrightarrow[26.9\ d]{\beta} U^{233} \xrightarrow[1.6 \times 10^5\ y]{\alpha}$$

In this work a gamma line associated with the Pa^{233} decay was used as a measure of the neutron capture, and it was therefore necessary to wait several days after activation for the Th^{233} to decay before chemical separation could be accomplished.

Dissolving thorium metal presents little difficulty, since it is vigorously attacked by hydrochloric acid, and the black residue produced will vanish upon the addition of a small amount of sodium fluosilicate.

A small amount of white residue (probably ThO_2) sometimes remains but dissolves when nitric acid is added and the solution is boiled.

Dissolving of sintered thorium-oxide pellets is more difficult but has been accomplished successfully and completely by boiling for one to four weeks in aqua regia (3 parts concentrated hydrochloric acid and 1 part concentrated nitric acid) to which a pinch of sodium fluosilicate (Na_2 Si F_6) has been added. The fluoride ion is necessary not only to help in dissolving the oxide but also to keep the protactinium in solution. Without the fluoride ion present the protactinium tends to adhere to the glassware. Care must be taken, however, to keep the amount of sodium fluosilicate to a minimum, since any excess will create an insoluble thorium-fluoride precipitate. For boiling pellets for long periods of time, as required in this investigation, it has been convenient to use the continuous refluxing apparatus shown in Fig. 2-9. Occasional evaporation almost to dryness was carried out, however, so that fresh aqua regia could be added.

Thorium and its daughters can be separated from protactinium by utilizing the ion-exchange properties of Dowex 21 K resin. The feed solution is approximately 14 N HCl from which protactinium is strongly absorbed by the resin. Thorium and its daughters are only weakly absorbed and appear in the feed effluent. The elutriant is 1.5 N HCl with about 5 drops of concentrated HF added to each 100 ml.

The solution of dissolved Th or ThO_2 is brought to the proper normality in HCl by successively evaporating almost to dryness and rediluting with concentrated HCl. These successive operations of evaporation and dilution are necessary to eliminate most of the nitric acid, since thorium forms absorbable nitrate complexes in a nitric acid solution. After the final dilution with concentrated HCl, the solution is not heated, since this will drive off HCl gas and thus reduce the acid concentration of the feed solution.

A column of resin about 6 inches in height contained in a 50 ml buret was used in the present work. This apparatus is shown in Fig. 2-10. A glass-wool plug at the bottom of the column supports the resin beads. The resin column is initially conditioned with concentrated HCl for several hours, and then the feed solution is poured in. The flow rate through the column is regulated to about one

drop per second. After all the feed solution has passed through the column, it is washed several times with concentrated HCl to remove any remaining thorium from the resin.

About 75 ml of elutriant has been found sufficient to remove the last trace of protactinium from the column. Thus, the protactinium could be eluted directly into a 100-ml volumetric flask for counting.

The uranium oxide samples employed in the Dancoff measurements were dissolved in HNO_3 and were transferred directly to 100-ml volumetric flasks and diluted for counting.

5.3. Counting Procedure

The flasks containing the protactinium solutions were positioned on a 3-inch sodium-iodide crystal by means of a lucite centering ring as shown in Fig. 2-11, and the gamma spectra was analyzed through the 400-channel analyzer system shown in Fig. 2-12. The protactinium gamma spectrum is shown in Fig. 5-1. There are strong photo peaks at 105 Kev and 310 Kev. The latter peak was used for quantitative measurement, and the counts in the central 11 channels of this peak were summed. This operation is facilitated by automatic digital printout of the counts stored in each channel of the analyzer. Prior to sample counting, the flasks were calibrated with a standard protactinium solution to obtain correction factors for slight variations in geometry and bottom thickness. The analyzer response was checked with a Cs^{137} standard before each count.

The flasks containing the uranium and neptunium resulting from neutron capture, were counted in a manner similar to that used for protactinium. The gamma line at 105 Kev associated with the Np^{239} decay was used as a measure of the neutron capture in uranium, and counts in the central 17 channels of this peak were summed. Background subtractions were employed to account for the presence of uranium.

Each gold monitor foil was counted on both sides in three different gas flow porportional counters of the type shown in Fig. 2-13. After the standard corrections the results were averaged to obtain the exposure normalization for each run.

The thin calibration samples deposited on Teflon planchets were also counted in the gas flow proportional counters and in addition some were gamma counted to obtain an independent measure of the thorium rod to dilute thorium specific activity ratio.

5.4. Reactivity Measurements

In the reactivity measurements, the test sample was first lowered to the center of the reactor where it rested on an aluminum spacer in the cadmium thimble. Criticality was established and maintained for approximately 10 minutes. To aid in establishing the exact critical condition, the steady-state signal from a gamma-compensated ion chamber was bucked out and the amplified time-dependent error signal was observed on a recorder. This indication, together with a special switching arrangement by which the control rod could be driven in minute increments, allowed rapid and precise stabilization.

With exact criticality established and the reactor stabilized, the test sample was withdrawn from the core and the reactor was allowed to approach an asymptotic period for a sufficient time to ensure less than 1% deviation from the asymptotic condition according to the criteria of Toppel.[4] The period was determined from the exponential power variation in the asymptotic region as indicated by the linear recorder chart. The reactivity worth for each sample was derived from the period measurements through the inhour equation.

Exactly similar measurements were made on the series of boron samples to obtain a calibration relative to the boron resonance integral.

Similar measurements were also made for samples of bismuth, aluminum, and aluminum oxide to provide data for correction for the effect of scattering by thorium and thorium oxide.

Fig. 5-1. Protactinium Gamma Spectrum

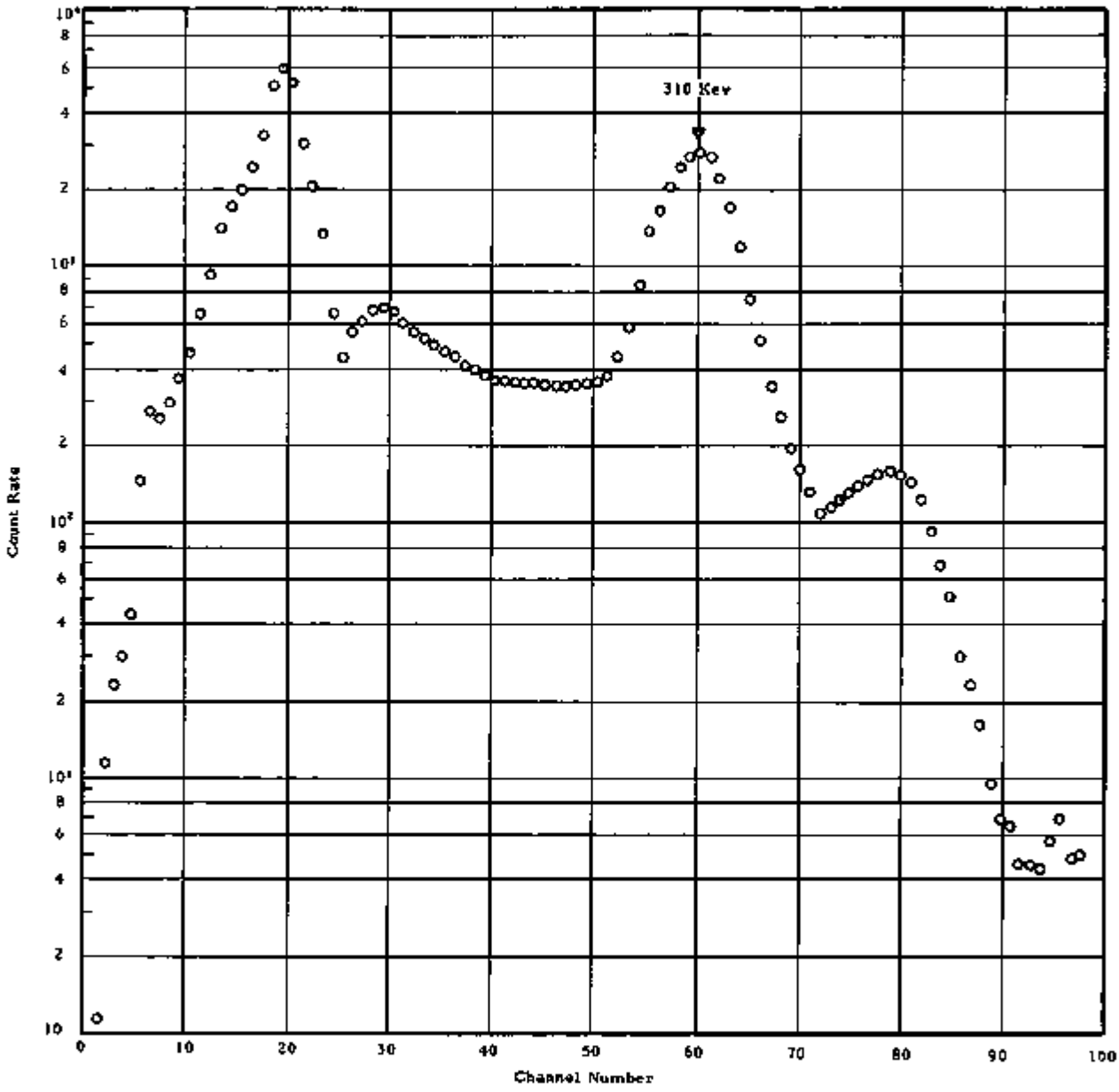

THIS PAGE
WAS INTENTIONALLY
LEFT BLANK

6. DATA ANALYSIS

6.1. Relative Sample Activities

Three independent activation measurements were carried out for each of the three rod sizes for both thorium metal and thorium oxide. Table 6-1 gives basic counting data and the results of sequential data reduction and normalization for thorium metal; Table 6-2 gives comparable data for thorium oxide. The relative exposures were determined from the activities of gold monitor foils. The gross count was corrected for background by automatic subtraction of a stored spectrum in the analyzer. The decay factor applies corrections for decay during and after exposure including the counting time. The flask factor is a small correction for variations in thickness and shape of the counting flasks. These factors were determined from measurements with accurately known quantities of a standard solution. The relative specific activities are corrected for all of these effects and, within the limits of uncertainty, are proportional to the effective resonance integrals in the LPR spectrum.

The relative specific activities in the thorium oxide temperature dependence measurements are given in Table 6-3. The sample diameter for all cases here is 0.266 in. The data treatment here was the same as described above.

Tables 6-4 and 6-5 give the activity data for the measurements of the Dancoff effect. The data treatment here also follows the method outlined above.

6.2. Activity Calibration

By the procedure described in Section 5.1, the ratio of the resonance capture per atom for a 0.158 inch diameter thorium rod sample to that of an infinitely thin sample (see Appendix A) was found to be 0.235 for the LPR spectrum. This capture ratio can be expressed

as follows:

$$\frac{\int_0^{\infty} \sigma_{a_1}(u)\,\phi(u)\,du}{\int_0^{\infty} \sigma_{a_\infty}(u)\,\phi(u)\,du} = \frac{\langle\phi_1\rangle I_1 + \int_{13.5}^{17.25} \sigma_{a_1}(u)\,\phi(u)\,du}{\langle\phi_\infty\rangle I_\infty} = 0.235 \qquad (6\text{-}1)$$

where I_1 is the resonance integral of the 0.158 inch thorium rod to lethargy of 13.5 or 13.71 ev, I_∞ is the thorium infinite dilution resonance integral to lethargy 17.25 or 0.322 ev, below which the flux is essentially zero, and the absorption weighted flux averages $\langle\phi_1\rangle$ and $\langle\phi_\infty\rangle$ are taken to lethargy 13.5 and 17. 5 respectively. The value of $\int_{13.5}^{17.25} \sigma_{a_1}(u)\,\phi(u)\,du$ is found to be 1.624 using the expression for σ_a given by Weitman[3] and the calculated flux spectrum. We have then,

$$I_1 = \frac{0.235\,\langle\phi_\infty\rangle\, I_\infty - 1.624}{\langle\phi_1\rangle} \qquad (6\text{-}2)$$

The value of I_∞, with reference to which these measurements are calibrated, is tentatively taken to be 86 barns in accord with recent measurements.[4,5] The flux averages are computed from the spectrum in Fig. 3-1 and the calculated energy distribution of the absorption. In the resolved resonance region the energy distribution of absorption was obtained from the exact treatment of the capture integral in Appendix B for the infinite dilution case and from the calculations of Nordhein[6] for the rod cases. The distribution below 17.6 ev was taken from the expression adopted by Weitman[3]. In the unresolved region from 1 to 15 kev the distribution was taken to be that of equally spaced levels with D = 20 ev, Γ_γ = 0.024 ev, and $\langle\Gamma_n^o\rangle$ = 0.0013 ev. Here a correction factor of 0.75 was applied to account for fluctuations in Γ_n^o. In the high energy region the distribution was taken from BNL-325. The values of $\langle\phi_\infty\rangle$ and $\langle\phi_1\rangle$ are found to be 1.006 and 1.063 respectively. From Equation 6-1 we then find I_1 = 17.60 barns for the effective resonance integral of the 0.158 inch rod in a 1/E flux to 13.71 ev.

Table 6-1. Thorium-Metal Activation Data

Sample diameter, cm	Counting sample mass, gm	Relative exposure	Net count	Decay factor	Flask factor	Relative specific activity	Average
0.401	0.2042	14.030	207843	1.594	1.026	1.1865	
	0.2065	14.7545	240216	1.4695	1.047	1.2130	1.2112 ±0.0138
	0.7333	5.2600	326621	1.396	1.044	1.2341	
1.008	1.3048	1.4484	108732	1.587	1.008	0.9203	
	1.3090	1.5288	124625	1.438	1.014	0.9080	0.9135 ±0.0036
	1.3103	1.5291	126088	1.398	1.037	0.9123	
2.934	11.0372	0.31683	162528	1.478	1.000	0.6869	
	11.1004	0.30878	165512	1.4345	1.010	0.6996	0.6928 ±0.0037
	11.1236	0.31588	172291	1.4025	1.006	0.6918	

Table 6-2. Thorium-Oxide Activation Data

Sample diameter, cm	Counting sample mass, gm	Relative exposure	Net count	Decay factor	Flask factor	Relative specific activity	Average
0.401	0.50945	7.0376	258612	1.852	1.027	1.5611	
	0.5535	6.9858	408877	1.298	1.035	1.6165	1.5862 ±0.0162
	0.4912	7.2611	252615	1.894	1.037	1.5818	
0.676	2.8190	1.1235	207313	1.547	1.045	1.2041	
	2.9600	1.1314	258957	1.298	1.018	1.1625	1.1835 ±0.0120
	3.0458	1.1385	120086	2.853	1.053	1.1839	
2.377	7.6290	0.43718	132111	1.850	1.044	0.8705	
	7.7790	0.41870	156483	1.512	1.032	0.8529	0.8694 ±0.0092
	7.8207	0.42758	85859	2.868	1.056	0.8848	

Table 6-3. Activity Data for the Doppler Coefficient Measurements

Temperature, °C	Counting sample mass, gm	Relative exposure	Gross count	Decay factor	Flask factor	Relative specific activity	Average
22	2.8878	1.1320	92445	3.5323	1.055	1.0538	1.0616 ±0.006
	3.0833	1.1135	96699	3.6403	1.043	1.0694	
200	2.9777	1.1018	81118	4.4755	1.040	1.1508	1.1508 ±0.009
500	2.9459	1.1187	91084	4.3625	1.015	1.2238	1.2238 ±0.009
800	3.0141	1.1256	135686	3.1078	1.038	1.2901	1.2986 ±0.006
	2.9729	1.1069	109097	3.7191	1.060	1.3070	

Table 6-4. Thorium Oxide Activation Data (Dancoff Measurement)

Center-to-center spacing	Counting sample mass, gm	Relative exposure	Net count	Decay factor	Flask factor	Relative specific activity	Average
0.422	10.5540	4.2811	209248	3.0210	1.041	2.9129	2.906 ± 0.046
	10.5483	4.3663	185207	3.5089	1.027	2.8982	
0.527	10.9582	4.4463	269323	2.6755	1.079	3.1914	3.104 ± 0.046
	10.6346	4.3444	219315	3.1004	1.025	3.0171	
0.738	11.0116	4.3068	280750	2.5937	1.053	3.2336	3.178 ± 0.046
	10.4234	4.3096	302942	2.2159	1.045	3.1233	
1.037	12.8139	4.3075	343583	2.5461	1.017	3.2237	3.224 ± 0.065

Table 6-5. Uranium Oxide Activation Data
(Dancoff Measurements)

Center-to-center spacing	Counting sample mass, gm	Relative exposure	Net count	Decay factor	Flask factor	Relative specific activity	Average
0.442	8.3385	4.3050	3875475	3.1932	1.025	11779	
	8.3734	0.40911	369400	3.2331	1.025	11912	11869 ± 128
	8.3748	0.41827	365597	3.2431	1.027	11587	
	8.2624	0.40746	377816	3.1689	1.029	12198	
0.527	8.2884	0.41750	379846	3.1624	1.037	11999	
	8.4436	0.41107	388817	3.0684	1.038	11893	12000 ± 80
	8.3578	0.41590	402905	3.0577	1.035	12227	
	8.2397	0.41719	386188	3.0748	1.032	11883	
0.738	8.3449	0.42425	387945	3.0913	1.044	11788	
	8.0952	0.41402	368931	3.2646	1.045	12518	12102 ± 152
	8.3346	0.42115	388368	3.1422	1.039	12041	
	8.1995	0.42528	401661	3.0175	1.041	12061	
1.037	8.3853	0.41612	402157	3.0621	1.047	12317	
	8.3512	0.40805	272378	4.4930	1.043	12486	12436 ± 59
	8.3313	0.41097	373218	3.2619	1.055	12504	

For the other metal and oxide rods the effective resonance integrals are found from the relation

$$\left(\frac{A_j}{A_1}\right)_{meas} = \frac{\langle\phi_j\rangle \; I_j \; + 1.624}{\langle\phi_1\rangle \; I_1 \; + 1.624} \qquad (6\text{-}3)$$

where $\frac{A_j}{A_1}$ is the activity per thorium atom relative to that of the 0.158 inch rod, $\langle\phi_j\rangle$ is the absorption weighted flux average computed as above, and I_j is the effective integral of the j^{th} rod to 13.71 ev in a 1/E flux. The results are given in Table 6-6.

Table 6-6. Effective Resonance Integrals to 13.71 ev in a 1/E Flux, Activation Results

Sample number j	Material	$\sqrt{S/M}$	Relative specific activity A_j/A_1	Average flux $\langle\phi_j\rangle$	Resonance integral, barns
1	Th	0.926	1	1.063	17.60
2	Th	0.584	0.7542	1.087	12.61
3	Th	0.342	0.5720	1.119	8.94
4	ThO_2	1.178	1.3096	1.047	23.88
5	ThO_2	0.806	0.9771	1.059	17.22
6	ThO_2	0.487	0.7178	1.088	11.92

6.3. Reactivity Coefficients

In the investigation of the dependence of the resonance integral on rod diameter the directly measured quantities are the gross reactivity worth of sample plus holder and the holder reactivity worth for each of the rod samples, the calibration samples, and the scattering samples. These data are listed in Table 6-7 along with the net reactivity and specific reactivity worths.

In the case of the boron calibration samples the holder correction includes the effect of the aluminum powder in which the boron particles were dispersed. The bismuth reactivity coefficient also includes a calculated 1% correction for resonance capture.

Table 6-7. Measured Reactivity Coefficients

Material	Diameter, cm	Mass, gm	Gross Reactivity, cents	Holder Reactivity, cents	Net Reactivity, cents	Specific Reactivity, cents/gm
Th	0.401	21.72	0.003	0.242	-0.239	-0.0110
Th	1.008	128.37	-0.774	0.250	-1.024	-0.00741
Th	2.934	1148.00	-5.796	0.307	-6.103	-0.00532
ThO_2	0.401	13.09	0.064	0.242	-0.178	-0.01360
ThO_2	0.676	48.50	-0.234	0.231	-0.465	-0.00959
ThO_2	2.377	359.39	-2.242	0.259	-2.501	-0.00696
ThO_2	2.934	690.68	-4.088	0.290	-4.378	-0.00634
Al	2.360	179.50	0.701	0.414	0.287	0.00160
Al_2O_3	3.095	355.40	0.112	0.423	-0.311	-0.000875
Bi	2.859	981.41	1.173	0.414	0.759	0.00078
B	0.457	0.05937	-0.030	0.175	-0.205	-3.453
B	0.457	0.09663	-0.149	0.176	-0.325	-3.363
B	0.457	0.16211	-0.366	0.179	-0.545	-3.362
B	0.457	0.30106	-0.783	0.183	-0.966	-3.209

In order to obtain the reactivity coefficient due to boron capture at infinite dilution it is necessary to make further corrections for self-shielding and boron scattering. The self-shielding factors $\langle P_o \rangle$ for each sample were computed as explained in Appendix C. These factors are given in Table 6-8 together with the infinite dilution reactivity coefficients. The average value of the infinite dilution reactivity coefficients is found to be -3.488¢/gm. The scattering contribution computed as described in Section 6.4 is -0.008¢/gm. When this correction is made the final infinite dilution reactivity coefficient due to boron capture is found to be -3.480¢/gm.

Table 6-8. Boron Self-Shielding Corrections

Boron mass, gm	Sample reactivity coefficient, cents/gm	Self-shielding factor $\langle P_o \rangle$	Infinite dilution reactivity coefficient, cents/gm
0.05937	-3.453	0.9835	-3.511
0.09663	-3.362	0.9736	-3.453
0.16211	-3.362	0.9568	-3.514
0.30106	-3.209	0.9234	-3.475

6.4. Scattering Corrections

The specific reactivity values listed in Table 6-7 for thorium and thorium oxide include a contribution due to scattering. In the case of thorium metal this correction is obtained from the bismuth reactivity coefficient by assuming that the scattering reactivity worth per atom is proportional to the potential scattering cross-section. The correction obtained on this basis is 0.00098¢/gm. In the case of thorium oxide an additional correction was necessary to account for the oxygen scattering. The reactivity coefficient for oxygen was obtained directly from the aluminum and aluminum oxide measurements and was found to be -0.00365¢/gm. These values yield a net scattering correction for thorium oxide of 0.00042¢/gm. A very small scattering correction (~0.2%) was also applied to the calibration samples to account for boron scattering. This was obtained from the oxygen coefficient under the

assumption that, for these light elements, the scattering reactivity per atom is proportional to $\xi \sigma_s$.

A general discussion of the effects of scattering on reactivity measurements is given in Appendix D. This treatment gives an explaination of the difference in the sign of the reactivity coefficients of oxygen and bismuth.

6.5. Reactivity Analysis

The deduction of the resonance integrals from the measured reactivity worths of the samples and the calibration standards is complicated by the fact that the energy distribution of the capture is not the same for thorium and boron, and by the fact that the fast fission in thorium contributes an experimentally inseparable positive reactivity effect. Therefore, for the thorium samples, the net reactivity, ρ, after scattering corrections is given by the importance weighted integral of the neutron removal minus production.

$$\rho = C\ N\ V \left[\int_0^\infty \sigma_{a_{eff}}(u) \phi(u) P(u)\, du + \int_0^\infty \sigma_f(u)\, \phi(u)\, P(u)\, du \right.$$

$$\left. - \langle P_f \rangle \int_0^\infty \nu(u)\, \sigma_f(u)\, \phi(u)\, du \right], \qquad (6\text{-}4)$$

where C is a constant, NV is the number of absorber atoms in the sample, σ_a is the (n, γ) cross section, $\phi(u)$ is the flux per unit lethargy at the sample position, P(u) is the neutron importance at the sample position and at lethargy u, σ_f is the fission cross section, $\langle P_f \rangle$ is the average of P(u) over the fission spectrum, and $\nu(u)$ is the average number of neutrons produced by a fission at lethargy u. The first integral may be written as

$$\int_0^\infty \sigma_{a_{eff}}(u)\ \phi(u)\ P(u)\, du = \langle \phi P \rangle \int_0^{13.5} \sigma_{a_{eff}}(u)\, du + \int_{13.5}^{17.25} \sigma_{a_{eff}}(u)\, \phi(u)\, P(u)\, du$$

$$= \langle \phi P \rangle\, I + \int_{13.5}^{17.25} \sigma_{a_{eff}}(u)\ \phi(u)\ P(u)\, du \qquad (6\text{-}5)$$

where $\langle \phi P \rangle$ is taken to lethargy 13.5 or 13.71 ev and I is the effective resonance integral over the same range. The last two integrals of Equation 6-4 and the last integral of Equation 6-5 are independent of the sample size and if the sum of these is represented by -K we then have

$$\rho = C\ N\ V\ [\langle \phi P \rangle\ I\ -K] \tag{6-6}$$

or

$$\rho/m = \frac{C'}{A}\ [\langle \phi P \rangle\ I\ -K] \tag{6-7}$$

where m is the sample mass and A is the atomic or molecular weight of the sample. The constant C' is determined from the boron reactivity measurements.

$$C' = \frac{A_B (\rho/m)_B}{\langle \phi P \rangle_B\ I_B} \tag{6-8}$$

where $\langle \phi P \rangle$ and I_B are taken to lethargy 17.25 or energy 0.322 ev to include all resonance capture in boron. From Equations 6-7 and 6-8 the resonance capture integral is then given by,

$$I = \frac{1}{\langle \phi P \rangle} \left[\langle \phi P \rangle_B\ I_B\ \frac{A}{A_B}\ \frac{(\rho/m)}{(\rho/m)_B} + K \right] \tag{6-9}$$

The average values of the product ϕP are computed from the calculated flux and importance functions given in Figs. 3-1 and 3-2 by numerical integration. The weight assigned to each group is the calculated fraction of the total resonance capture which occurs in that group. For the boron samples this distribution is proportional to 1/v and the factor $\langle \phi P \rangle_B$ is found to be 0.3707. For the thorium and thorium oxide samples the distributions were obtained as explained in Section 6.2. The factor I_B is the resonance integral of boron from 0.322 ev and is given by

$$I_B = \int_{0.322}^{\infty} \sigma_a(E)\ \frac{dE}{E}$$

$$= 4.24 \text{ barns} \tag{6-10}$$

where

$$\sigma_a(E) = \sigma_a(0.0253)\sqrt{\frac{0.0253}{E_{ev}}}$$

and

$$\sigma_a(0.0253) = 761 \text{ barns}$$

The term K is given by

$$K = \int_0^{\infty} \sigma_f(u)\,\phi(u)[\nu(u)\langle P_f\rangle - P(u)]\,du - \int_{13.5}^{17.25} \sigma_{a_{eff}}(u)\,\phi(u)\,P(u)\,du$$

$$= 1.08 - 0.66 = 0.42 \qquad (6\text{-}11)$$

where

$$\nu(E) = 1.877 + 0.177\,E_{mev} \qquad (6\text{-}12)$$

as reported by Conde and Starfelt.[7] $\langle P_f\rangle$ is the importance function averaged over the fission spectrum, and $\sigma_{a_{eff}}(u)$ is taken from the work of Weitman.[3] The final expressions for Equation 6-9 for the resonance integrals of thorium and thorium oxide to 13.71 ev in a 1/E flux are,

$$I_{Th} = \frac{970\,\rho/m + 0.42}{\langle\phi P\rangle} \qquad (6\text{-}13)$$

$$I_{ThO_2} = \frac{1104\,\rho/m + 0.42}{\langle\phi P\rangle} \qquad (6\text{-}14)$$

The corrected specific reactivities, the $\langle\phi P\rangle$ factors, and the resonance integrals to 13.71 ev are listed in Table 6-9.

Table 6-9. Effective Resonance Integrals to 13.71 ev in a 1/E Flux, Reactivity Results

Material	$\sqrt{S/M}$	Corrected specific reactivity, cents/gm	$\langle \phi P \rangle$	Resonance integral, barns
Th	0.933	-0.01198	0.733	16.43
Th	0.594	-0.00839	0.765	11.19
Th	0.359	-0.00630	0.805	8.11
ThO_2	1.186	-0.01402	0.713	22.30
ThO_2	0.815	-0.01001	0.727	15.78
ThO_2	0.511	-0.00738	0.764	11.21
ThO_2	0.459	-0.00676	0.771	10.22

7. RESULTS AND DISCUSSION

7.1. Geometric Dependence

The results of the activation measurements of the geometric dependence are shown in Fig. 7-1 for both the metal and oxide cases. As explained in Section 6.2 these results do not include any "1/v" or negative energy resonance contribution below 13.71 ev. The calibration standard is infinitely dilute thorium for which the total resonance integral in a 1/E flux to 0.322 ev is tentatively taken as 86 barns. This value is to some extent arbitrary since measured values ranging from 67±5 to 106±10 barns (above 1/v) have been reported.[8,2] However, the choice of 86 barns to 0.322 ev corresponds to about 83 barns for the above 1/v contribution of the positive energy resonances and is consistent with the most recent measurements.[4,5] The uncertainty in the absolute calibration is estimated to be about ±5%.

For both the metal and oxide cases the data are very well correlated by a linear function of $\sqrt{S/M}$. Least squares fits to the data give

$$I_{Th} = 3.91 + 14.81 \sqrt{S/M} \quad \text{barns} \tag{7-1}$$

$$I_{ThO_2} = 3.41 + 17.32 \sqrt{S/M} \quad \text{barns} \tag{7-2}$$

The uncertainty due to random experimental errors is negligible in comparison with the 5% calibration uncertainty assigned. There is, however, an additional uncertainty of about 0.3 barns arising from the removal of the "1/v" and negative energy resonance contribution.

The results of the reactivity measurements of the geometric dependence are shown in Fig. 7-2. Least squares fits to the data give:

$$I_{Th} = 2.75 + 14.56 \sqrt{S/M} \quad \text{barns} \tag{7-3}$$

$$I_{ThO_2} = 2.66 + 16.45 \sqrt{S/M} \quad \text{barns} \tag{7-4}$$

Here the calibration is based on the 761 ± 2 barn absorption cross section of natural boron at 0.0253 ev. In this case the major source of uncertainty arises from the fact that the interpretation of the experimental data is strongly dependent on the calculated neutron importance function inside the cadmium tube. This function varies very rapidly with energy near the cadmium cut-off where the boron capture cross-section is most significant. The limits of error in the reactivity calibration due to this effect are very difficult to estimate because of the nature of the multigroup diffusion program used in obtaining the flux adjoints. A 10% overall uncertainty in the calibration is assigned here. An additional uncertainty of about 0.5 barns is present because of scattering corrections and corrections for the capture below 13.71 ev in thorium. The random errors in the measured reactivity coefficients are negligible compared to the above systematic errors.

The reactivity data in Fig. 7-2 are in good agreement with the activation data in regard to the $\sqrt{S/M}$ dependence and relative capture in metal and oxide at a given S/M value. The absolute values are systematically about 10% lower here than for the activation measurements but the discrepancy is well within the uncertainties involved in the calibration of the two experiments. The comparison of the two methods indicates that although they yield mutually consistent results the activation method is capable of significantly higher accuracy and this condition will prevail until more accurate programs are available for calculating the detailed energy dependence of the neutron importance function.

For purposes of comparison with previous measurements the activation results are accepted as being the most reliable and no further reference to the reactivity results will be made except to note that they are in good agreement with previous similar measurements made at this laboratory[10] when the same analysis procedure (see Section 6.5), including the effect of the cadmium thimble on the importance function, is employed. Fig. 7-3 shows a comparison of the present results with other recent measurements and Fig. 7-4 shows a similar comparison for thorium oxide. In the thorium metal case the present results and those of Hellstrand and Weitman are in good agreement over the entire mutual range of measurement. The discrepancy

between the present work and that of Moore, et al, is within the combined estimated uncertainties of the two measurements but the discrepancy would be greatly reduced if the correction of about 16% suggested by Weitman [3] is applied to Moore's results to account for the variation of the neutron importance function. The results of Rothman and Ward lie from 1.5 to 3 barns lower than the present results but this discrepancy is primarily due to their subtraction of too large a correction for the epi-cadmium "1/v" contribution. If a correction of 1.5 barns rather than 3.6 barns is made the results will be brought into satisfactory agreement.

In the thorium oxide case the results of the present work are in best agreement with the measurements of Weitman, the discrepancy here being everywhere well within the experimental uncertainties. In comparison with the measurements of Moore, et al and with those of Thie * the discrepancies are considerably larger over most of the range of measurement. Both of these measurements, however, were made by reactivity methods and the inherent uncertainties in analysis and calibration are such that the apparent discrepancies are of doubtful fundamental significance.

7.2. Temperature Dependence

The thorium oxide sample used in the temperature dependence measurements has a $\sqrt{S/M}$ value of 0.806 and from Fig. 7-4 its resonance integral is found to be 17.37 barns at room temperature or 22°C. The resonance integral at higher temperatures is obtained from the measured activity ratios through Equation 6-3. For this purpose the absorption weighted flux average $\langle\phi\rangle$ is assumed to be independent of sample temperature and the room temperature value $\langle\phi\rangle = 1.059$ is used. From Equation 6-3 we then find

* A "1/v" part of 1.5 barns has been subtracted from Thie's results of $I = -2.2 + 25.3 \sqrt{S/M_{ThO_2}}$

$$\frac{I(T)}{I(T_o)} = \frac{20.02\ A/A_o - 1.624}{18.396} \qquad (7\text{-}5)$$

The results are given in Table 7-1 and Fig. 7-5. A reasonable good empirical representation of the data is given by the relation,

$$I(T) = I(T_o)[1 + 0.016\ (\sqrt{T} - \sqrt{T_o})] \qquad (7\text{-}6)$$

where T is the Kelvin absolute temperature. No previous direct measurements of the temperature dependence have been reported except for some reactivity measurements made at this laboratory [19] in 1958. In these measurements it was found that

$$\frac{I + (1/v)}{I_o + (1/v)} = 1 + 0.17 \log \frac{T}{296} \qquad (7\text{-}7)$$

where (1/v) is the epi-cadmium contribution to the resonance integral below 13.71 ev, T is the Kelvin absolute temperature and the log function is the natural logarithm. Although these were reactivity measurements they were relative measurements for a given rod at various temperatures and hence are independent of calibration standards and importance function variations. The results may therefore be expected to be directly comparable to those of the present measurements and, in fact, the agreement of Equation 7-7 with the present measured values is within about 1% over the entire range of measurement. This confirmation by an independent technique indicates that the empirical representation in Equation 7-6 is reliable to within a few percent at most for uniformly heated thorium oxide rods of practical size for water moderated reactors.

Table 7-1. Variation of the Effective Resonance Integral of Thorium Oxide with Temperature

Temperature °C	$\sqrt{T} - \sqrt{T_o}$ $(°K)^{1/2}$	A/A_o	I/I_o
22	0	1	1
200	4.58	1.084	1.091
500	10.64	1.153	1.166
800	15.59	1.223	1.243

Fig. 7-1. Geometric Dependence, Activation Results

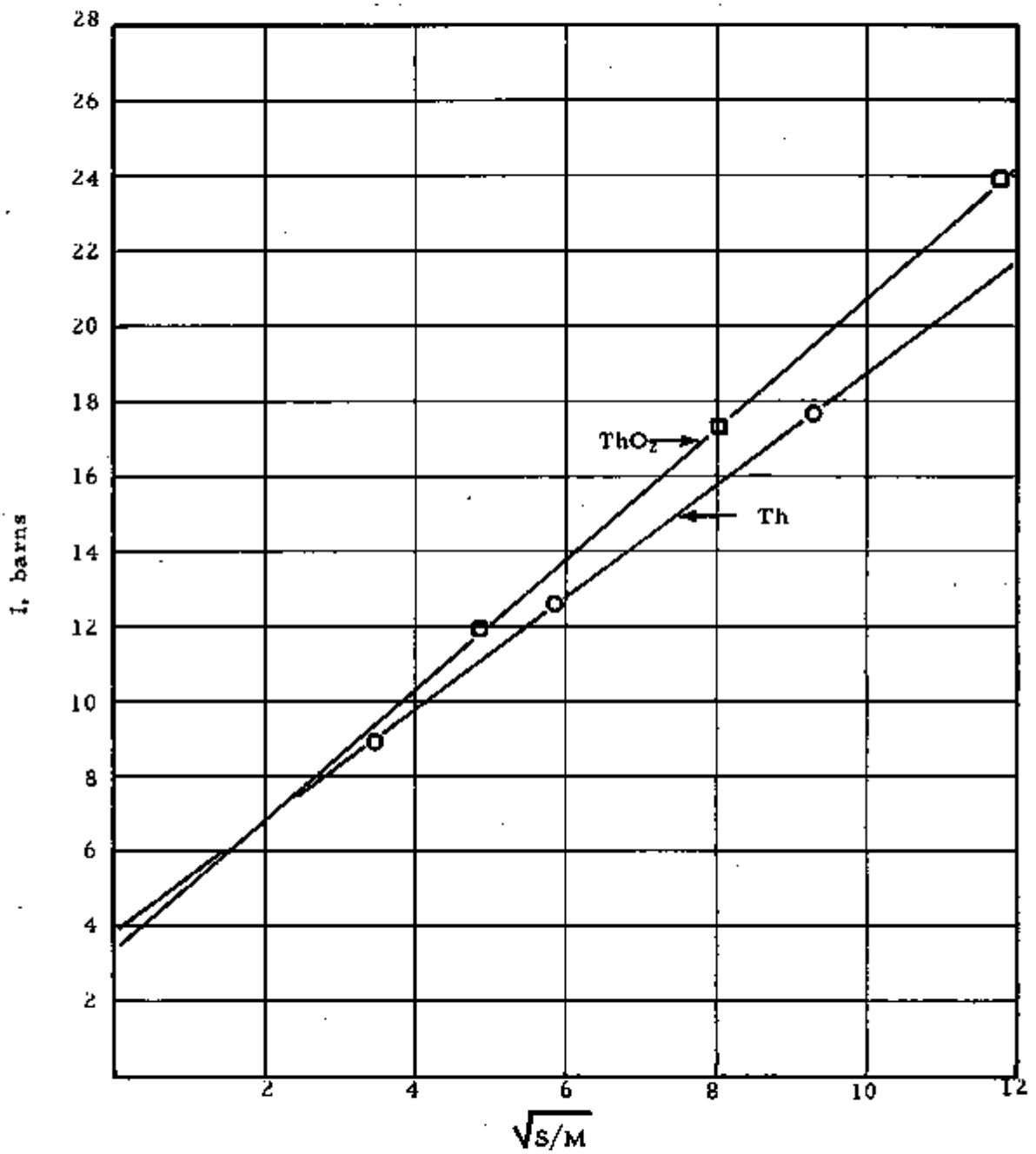

Fig. 7-2. Geometric Dependence, Reactivity Results

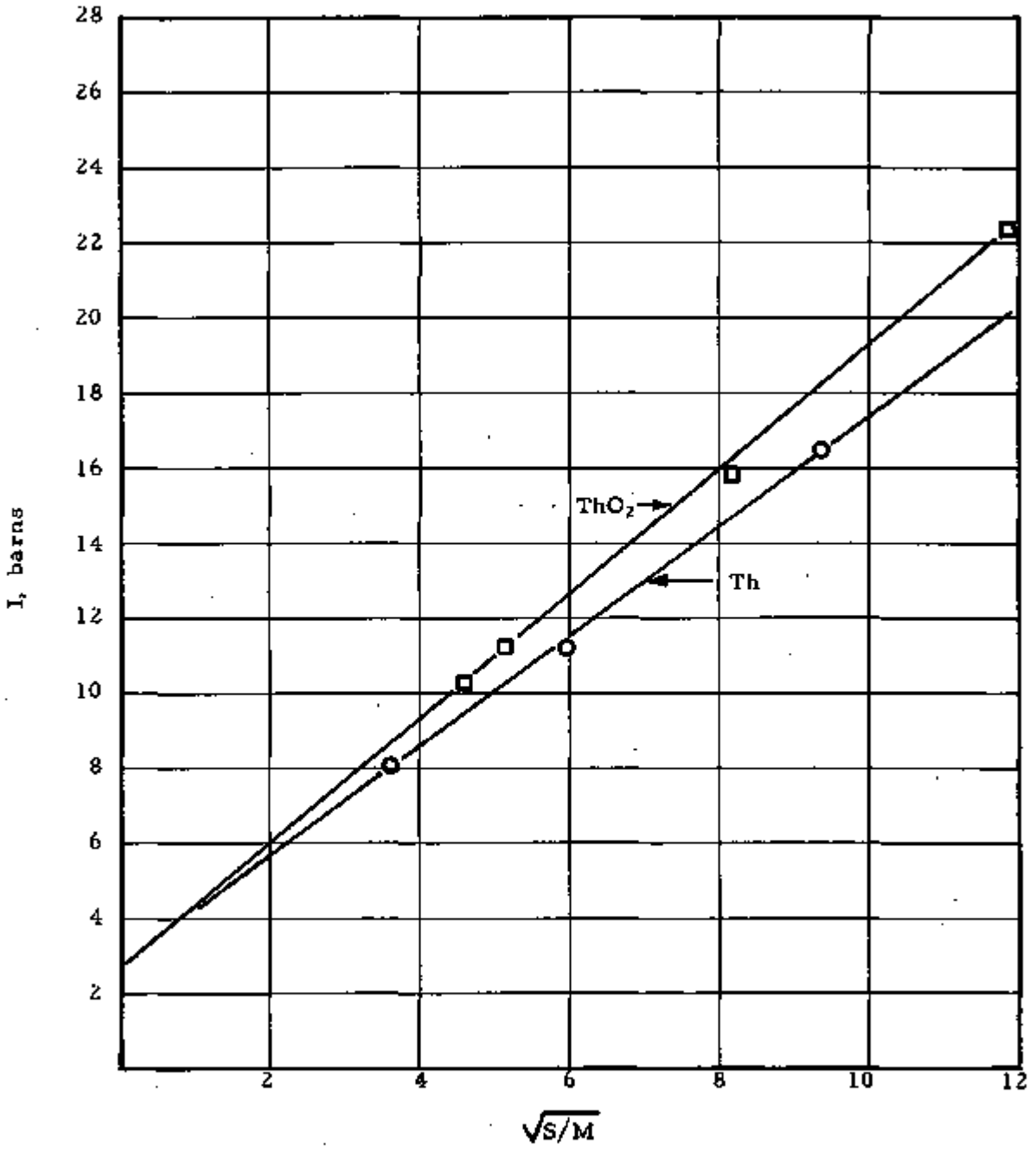

Fig. 7-3. Comparison of Thorium Metal Results with Other Recent Measurements

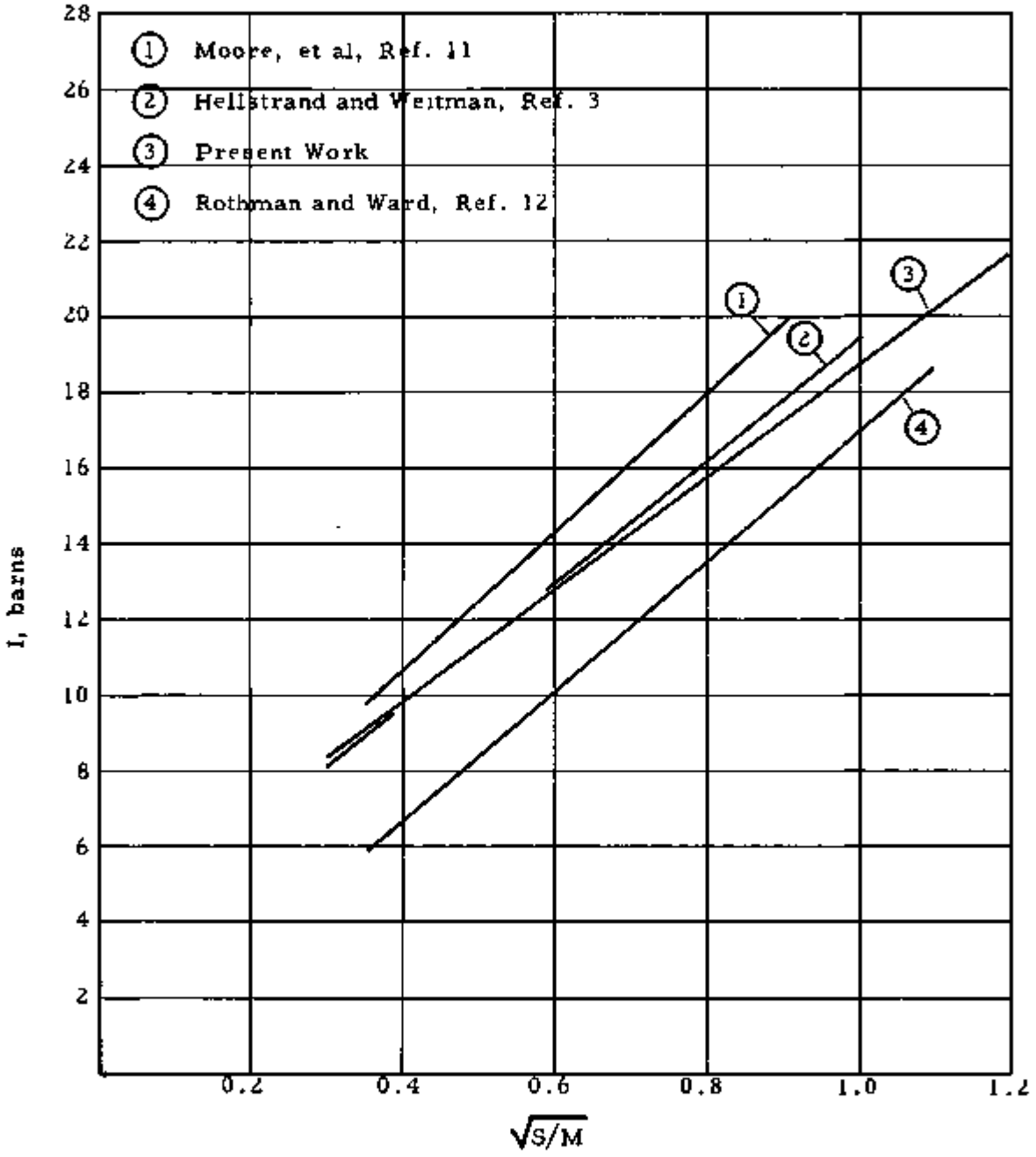

Fig. 7-4. Comparison of Thorium Oxide Results with Other Recent Measurements

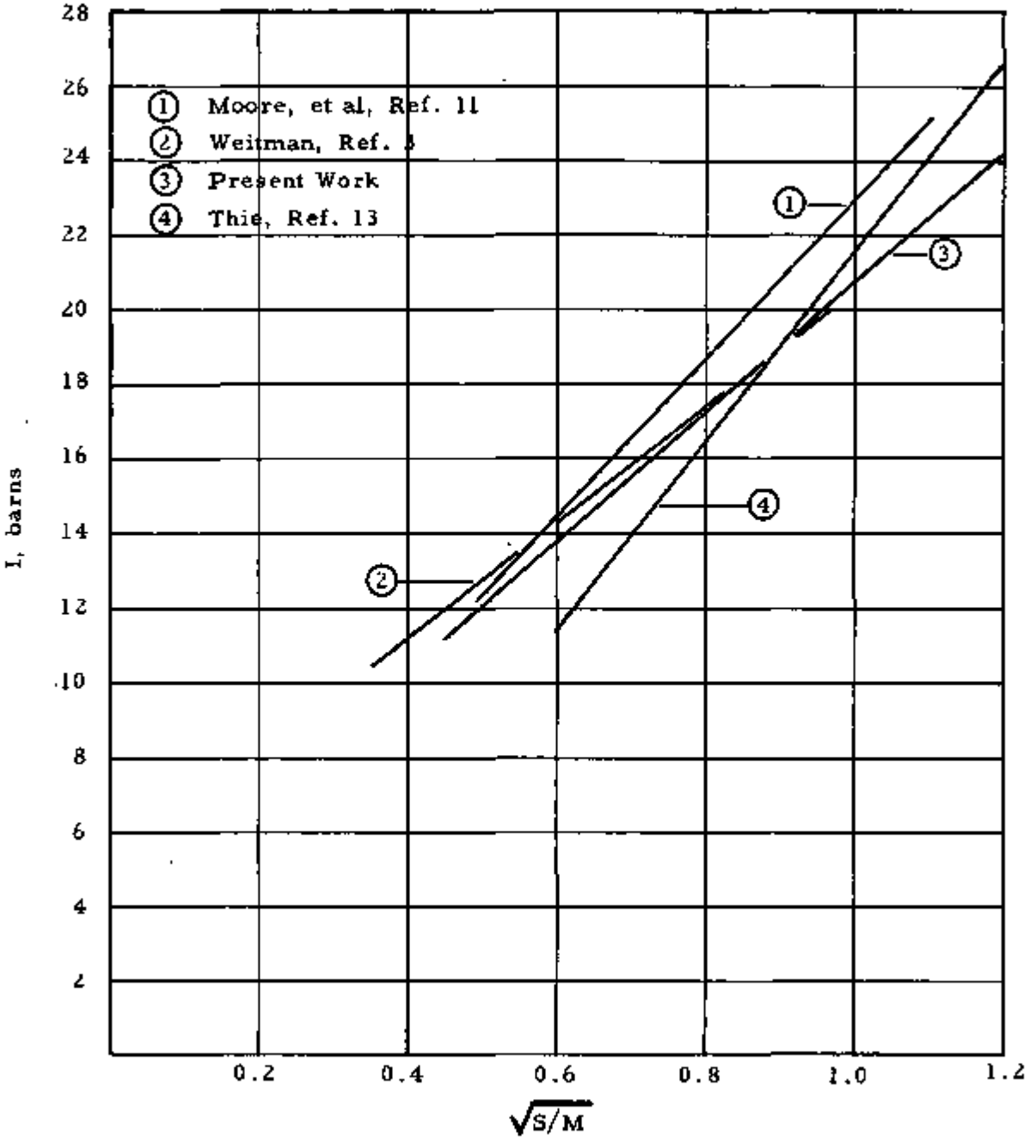

Fig. 7-5. Temperature Dependence of the Effective Resonance Integral of ThO_2

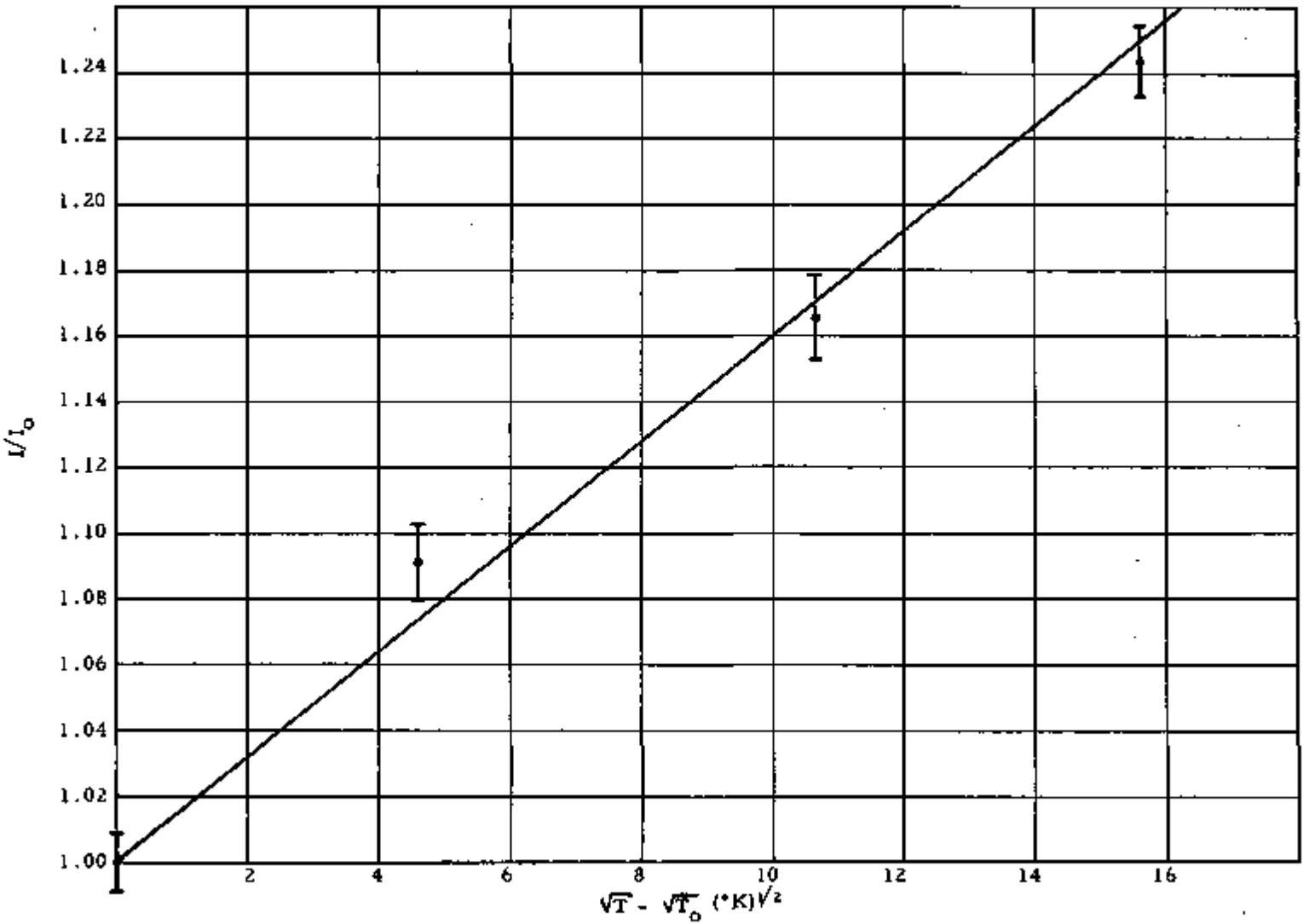

7.3. Dancoff Effect

These measurements constitute a direct experimental test of the original treatment of Dancoff and Ginsburg [14] to account for the mutual shielding of parallel rods with absorbing resonances. This theory provides a formula for computing the fractional reduction (c) in the resonance absorption of a rod having a narrow black resonance, caused by an identical parallel neighboring rod. Since the absorption in a black resonance necessarily occurs at the rod surface the factor (c) may be regarded as operating to reduce the physical surface (s) in an empirical representation of the resonance integral as a function of S/M. Accordingly, it may be expected that the ratio of the resonance integral of a shielded rod to that of an unshielded rod is given by

$$\frac{I}{I_o} = \frac{A+B\sqrt{\frac{S(1-c)}{M}}}{A+B\sqrt{S/M}} \tag{7-8}$$

where A and B are empirical constants as, for example, in Equation 7-2.

The ratio I/I_o is related to the measured activity ratio A/A_o by the expression

$$\frac{A}{A_o} = \frac{\langle\phi\rangle I + \int_{u_o}^{\infty} \sigma_a(u)\,\phi(u)\,du}{\langle\phi\rangle I_o + \int_{u_o}^{\infty} \sigma_a(u)\,\phi(u)\,du} . \tag{7-9}$$

Here the values of $\langle\phi\rangle$ and the integrals are found as explained in Section 6.2 and the value of I_o is taken from the most recent data. The value of u_o which corresponds to the upper energy limit of the "1/v" part is taken as 13.50 (13.71 ev) for thorium oxide and 15.75 (1.44 ev) for uranium oxide. The lower energy limit (at which the flux inside the cadmium tube vanishes) occurs at lethargy 17.25 (0.322 ev) and is the same for both cases. For the thorium oxide sample the numerical values are $\langle\phi\rangle = 1.068$, $I_o = 15.17$, and $\int_{13.50}^{17.25} \sigma_a(u)\,\phi(u)\,du = 1.624$.

In the uranium oxide case the values are $\langle\phi\rangle = 1.039$, $I_o = 20.40$, and $\int_{15.75}^{17.25} \sigma_a(u)\,\phi(u)\,du = 0.792$. The experimental resonance integral ratios are then given by

$$\frac{I}{I_o} = \frac{A}{A_o} - 0.100\left(1 - \frac{A}{A_o}\right) \qquad ThO_2$$

$$\frac{I}{I_o} = \frac{A}{A_o} - 0.037\left(1 - \frac{A}{A_o}\right) \qquad UO_2$$

The results for each lattice spacing are given in Tables 7-2 and 7-3 for the thorium oxide and uranium oxide cases, respectively, together with the comparable theoretical ratios.

In computing the theoretical ratios by Equation 7-8 the values of c were found by interpolation of the results of Carlvik [15]. For purposes of obtaining the mean-free-path parameter needed for the use of Carlvik's tables the rod cladding was regarded as homogenized in the moderator portion of the unit cell. In the thorium oxide case the isolated rod resonance integral is taken as given in Equation 7-2. For the uranium oxide case the results of Reference 1 are used after renormalization from 265 to 280 barns for the infinite dilution resonance integral of U^{238} in accordance with the presently accepted value of that quantity. The renormalized expression for the isolated rod resonance integral is $I_{UO_2} = 0.85 + 29.8\sqrt{S/M}$.

The experimental and calculated ratios are in agreement within the limits of experimental error and the uncertainty in the use of Carlvik's tables for a rod with cladding. These results therefore constitute a direct confirmation of the validity and practical usefulness of the Dancoff treatment where the factor (1-c) is regarded as a surface reduction operator in accord with the "black absorber" hypothesis of the theory.

Table 7-2. Comparison of Measured and Calculated Dancoff Shielding Effects for Thorium Oxide

Center-to-center spacing, in.	Relative specific activity, A	A/A_o	I/I_o exp.	c	I/I_o theor.
0.442	2.906±0.046	0.898±0.016	0.887±0.016	0.1255	0.950
0.527	3.104±0.046	0.952±0.016	0.947±0.016	0.0925	0.964
0.738	3.178±0.046	0.982±0.016	0.980±0.016	0.0505	0.980
1.037	3.224±0.065	0.996±0.022	0.996±0.022	0.0260	0.990
∞	3.236±0.025	1	1	0	1

Table 7-3. Comparison of Measured and Calculated Dancoff Shielding Effects for Uranium Oxide

Center-to-center spacing, in.	Relative specific activity, A	A/A_o	I/I_o exp.	c	I/I_o theor.
0.442	11869±128	0.947±0.014	0.945±0.014	0.1225	0.937
0.527	12000±80	0.958±0.011	0.956±0.011	0.0900	0.956
0.738	12102±152	0.966±0.015	0.966±0.015	0.0495	0.976
1.037	12436±59	0.993±0.011	0.993±0.011	0.0255	0.988
∞	12529±122	1	1	0	1

APPENDIX A

SELF-SHIELDING OF THE THIN ACTIVITY CALIBRATION SAMPLES

It is shown here that the thorium calibration samples used in the activation measurements are thin enough so that self shielding is negligible.

For a given resonance the effective resonance capture integral is

$$I = \int \sigma_a(E)\, P_o(E)\, \frac{dE}{E}$$

where $P_o(E)$ is the average escape probability given in the rational approximation by

$$P_o(E) = \frac{1}{1 + t\Sigma_a(E)}$$

With this approximation and the substitution $x = \frac{2}{\Gamma}(E-E_o)$ in the Breit-Wigner expression for $\Sigma_a(E)$, the effective resonance integral becomes,

$$I \approx \frac{\Gamma\, \Sigma_{a_o}}{N E_o} \int_0^\infty \frac{dx}{1 + t\Sigma_{a_o} + x^2}$$

$$\approx \frac{\pi\, \sigma_{a_o}\, \Gamma}{2E_o \sqrt{1 + t\Sigma_{a_o}}}$$

In the case of an infinitely thin foil $P_o = 1$ and

$$I_\infty = \frac{\pi\, \sigma_{a_o}\, \Gamma}{2E_o}$$

The resonance integral ratio for the finite thickness to the infinitely thin case is then given by

$$\frac{I}{I_\infty} \approx \frac{1}{\sqrt{1 + t\Sigma_{a_o}}}$$

$$\approx 1 - \frac{1}{2}\, t\Sigma_{a_o}$$

For the thorium deposit of 0.20 mg/cm^2 used for the calibration samples this gives

$$\frac{I}{I_\infty} \approx 0.998$$

for the resonance at 21.9 ev. The self-shielding of the higher energy resonances is generally even less significant and Doppler broadening reduces the effect still further. It is concluded therefore that the departure of the calibration samples from the infinitely thin condition is negligible.

APPENDIX B

EXACT EVALUATION OF THE RESOLVED RESONANCE CAPTURE INTEGRAL

The shape of an isolated s-wave (n,γ) resonance is given by the Breit-Wigner single level formula

$$\sigma_\gamma = \pi g \frac{\hbar^2}{2mE}\left(\frac{m + M}{M}\right)^2 \frac{\Gamma_n \Gamma_\gamma}{(E - E_o)^2 + \frac{\Gamma^2}{4}} \qquad \text{(B-1)}$$

where E_o and Γ_γ may be regarded as constant, but Γ_n and Γ are significantly dependent on the incident neutron energy E. The factor $(m + M)/M$ is the ratio of the mass of the compound nucleus to that of the target nucleus and arises from the transformation from the center-of-mass coordinate system to the laboratory coordinate system (the target nucleus is regarded as free and at rest). In computations of the resonance integral

$$RI = \int_{E_1}^{E_2} \sigma_\gamma(E) \frac{dE}{E} \qquad \text{(B-2)}$$

it is customary to elude the mathematical complications by symmetrizing the integrand, i.e., by ignoring the energy dependence everywhere except in the rapidly varying term $(E - E_o)^2$ in the denominator of Equation B-1 and extending the integration over the range $(-\infty, \infty)$. In this approximation the omitted capture on the low-energy side of the resonance is roughly compensated by the addition of an integral over a straight 1/v cross section. An improved approximation given by Story,* neglects the energy dependence only in the Γ^2 term in the denominator of Equation B-1. In this case the 1/v contribution is included as part of the integral.

---

* Story, J. S., Nuclear Data Series, Atomic Energy Research Establishment, AERE T/R 2389, Harwell, Great Britain, 1957.

It is possible, however, to obtain the following closed analytical expression for the resonance integral in which the complete energy dependence is retained:

$$RI = g\frac{\pi\hbar^2\,\Gamma_n^o\,\Gamma_\gamma}{2m}\left(\frac{m+M}{M}\right)^2\int_{E_1}^{E_2}\frac{dE}{E^{3/2}\left[\left(E-E_o\right)^2+\frac{1}{4}\left(\Gamma_n^o\sqrt{E}+\Gamma_\gamma\right)^2\right]}$$

$$= K\left[A\log U + B\tan^{-1}V + C\log W + D\tan^{-1}X + FE^{-1/2}\right]_{E_1}^{E_2} \qquad (B\text{-}3)$$

where

$$K = \frac{8\pi g\hbar^2 E_o^2\,\Gamma_n^o\,\Gamma_\gamma}{m\left(4E_o^2+\Gamma_\gamma^2\right)\left(\Gamma_\gamma^2-E_o\Gamma_n^{o2}\right)}\left(\frac{m+M}{M}\right)^2$$

$$A = \frac{E_o^2\left(\beta P - \alpha Q\right)}{\mu\left(4E_o^2+\Gamma_\gamma^2\right)}$$

$$B = \frac{2E_o^2\left(\alpha P + \beta Q\right)}{\mu\left(4E_o^2+\Gamma_\gamma^2\right)}$$

$$\mu = \sqrt{\left(2E_o-\frac{\Gamma_n^{o2}}{8}\right)^2+\Gamma_\gamma^2}$$

$$\alpha = \sqrt{\mu+\left(2E_o-\frac{\Gamma_n^{o2}}{8}\right)}$$

$$\beta = \sqrt{\mu-\left(2E_o-\frac{\Gamma_n^{o2}}{8}\right)}$$

$$P = \frac{\Gamma_\gamma}{E_o}\left[\left(1+\frac{\Gamma_\gamma^2}{4E_o^2}\right)+\frac{\Gamma_n^{o^2}}{4E_o}\left(1+\frac{\Gamma_\gamma^2}{2E_o^2}-\frac{\Gamma_n^{o^2}}{4E_o}\right)\right]$$

$$Q = \frac{\Gamma_n^{o^2}}{4E_o}\left[3+5\frac{\Gamma_\gamma^2}{4E_o^2}+\frac{\Gamma_n^{o^2}\Gamma_\gamma^2}{16E_o^3}-\frac{\Gamma_n^{o^2}}{4E_o}\right]-\frac{\Gamma_\gamma^2}{2E_o^2}\left(1+\frac{\Gamma_\gamma^2}{4E_o^2}\right)$$

$$C = \frac{\Gamma_n^o\,\Gamma_\gamma\left(\Gamma_\gamma^2 - E_o\,\Gamma_n^{o^2}\right)}{4E_o^2\left(4E_o^2+\Gamma_\gamma^2\right)}$$

$$D = \frac{-2E_o\Gamma_n^o}{4E_o^2+\Gamma_\gamma^2}\left(1+3\frac{\Gamma_\gamma^2}{4E_o^2}+\frac{\Gamma_n^{o^2}\Gamma_\gamma^2}{16E_o^3}-\frac{\Gamma_n^{o^2}}{4E_o}\right)$$

$$F = \frac{E_o\Gamma_n^{o^2}-\Gamma_\gamma^2}{2E_o^2}$$

$$U = \frac{\left(E-\frac{\mu}{2}+\frac{\Gamma_n^{o^2}}{16}\right)^2+\left(\beta\sqrt{E}+\frac{a\,\Gamma_n^o}{4}\right)^2}{\left[E-a\sqrt{E}+\frac{\mu}{2}+\frac{\Gamma_n^o}{4}\left(\beta+\frac{\Gamma_n^o}{4}\right)\right]^2}$$

$$V = \frac{-\left(\beta\sqrt{E}+\frac{a\Gamma_n^o}{4}\right)}{E-\frac{\mu}{2}+\frac{\Gamma_n^{o^2}}{16}}$$

$$W = \frac{\left(E-E_o\right)^2+\frac{1}{4}\left(\Gamma_n^o\sqrt{E}+\Gamma_\gamma\right)^2}{E^2}$$

$$X = \frac{\Gamma_n^o \sqrt{E} + \Gamma_\gamma}{2(E_o - E)}$$

$$o \leqq \tan^{-1} V \leqq \pi$$

$$o \leqq \tan^{-1} X \leqq \pi$$

If other interactions with energy-dependent widths Γ_i are effective, then Γ_γ must be replaced by $\Gamma_\gamma + \sum \Gamma_i$ everywhere except in the numerator of the factor K.

The apparent singularity arising from the factor $\Gamma_\gamma^2 - E_o \Gamma_n^{o^2}$ in the denominator of K causes no difficulty because this factor cancels from the coefficients C and F, and the remainder of the expression in brackets is zero when $\Gamma_\gamma^2 = E_o \Gamma_n^{o^2}$. Also, there is no difficulty in using Equation B-3 to obtain the contribution of a negative energy resonance since the formula is expressed so that only real numbers appear as input parameters or derived auxiliary parameters. We note also that the Story approximation, in a general form suitable for negative energy resonance, may be obtained from Equation B-3 by putting $\Gamma_n^o = 0$ and $\Gamma_\gamma = \Gamma$ everywhere except in the numberator of K.

Table B-1 gives the resonance integral of each resonance calculated by Equation B-3 to 0.4 ev for the zero temperature, infinite dilution, thorium case. The value of Γ_γ was taken as 0.024 ev for all resonances and the other resonance parameters are given in the table. The symmetrical resonance integrals over the range $(-\infty, \infty)$ are given for comparison.

Table B-1. Resolved Resonance Integrals of Thorium

Resonance energy, ev	Reduced neutron width, ev	Symmetrical resonance integral, barns	Exact resonance integral, barns
21.9	0.00051	18.485	18.545
23.6	0.00085	25.834	25.919
59.6	0.00060	4.464	4.475
69.7	0.00470	12.519	12.572
113.1	0.00104	2.416	2.421
121.0	0.00168	2.912	2.919
128.5	0.0000089	0.025	0.025
129.4	0.000265	0.653	0.654
146.2	0.00000827	0.019	0.019
154.6	0.0000180	0.038	0.038
170.8	0.00445	2.378	2.387
193.0	0.00101	0.971	0.973
196.8	0.0000093	0.014	0.014
199.8	0.00064	0.672	0.673
203.0	0.000003	0.004	0.004
221.8	0.00154	0.974	0.976
252.3	0.00151	0.770	0.771
264.0	0.00092	0.540	0.541
286.8	0.00122	0.551	0.552
306.5	0.00114	0.474	0.475
330.4	0.00302	0.625	0.626
343.3	0.00162	0.462	0.463
366.7	0.00183	0.433	0.434
371.0	0.00125	0.357	0.357
402.8	0.00045	0.165	0.165
413.4	0.000005	0.002	0.002
456.4	0.000005	0.002	0.002
465.0	0.00209	0.296	0.296
491.0	0.00226	0.275	0.275
513.0	0.000154	0.047	0.047

Table B-1. (Cont'd)

Resonance energy, ev	Reduced neutron width, ev	Symmetrical resonance integral, barns	Exact resonance integral, barns
531.5	0.00065	0.133	0.134
543.0	0.000043	0.013	0.013
573.0	0.00104	0.152	0.152
581.0	0.000066	0.018	0.018
601.5	0.00045	0.085	0.085
621.5	0.00020	0.044	0.044
660.5	0.00124	0.128	0.128
669.0	0.00066	0.091	0.091
679.5	0.0048	0.178	0.179
692.0	0.00148	0.127	0.127
705.0	0.00068	0.085	0.085
717.5	0.00094	0.097	0.098
746.0	0.00585	0.153	0.154
783.0	0.00036	0.047	0.047
810.0	0.0044	0.125	0.126
848.0	0.00079	0.067	0.067
872.0	0.00034	0.038	0.038
896.0	0.0010	0.068	0.068
950.0	0.0013	0.068	0.068
970.0	0.00024	0.025	0.025
990.0	0.00076	0.050	0.050
998.0	0.0022	0.073	0.073
			79.481

APPENDIX C

SELF-SHIELDING CORRECTIONS FOR BORON CALIBRATION SAMPLES

For monoenergetic neutrons, the shielding factor for cylindrical absorbers is given by Case, de Hoffman and Placzek * as

$$P_o = 1 - \frac{4}{3} r\Sigma_a + 1/2 (r\Sigma_a)^2 \left[\log \left(\frac{2}{r\Sigma_a}\right) + \frac{5}{4} - \gamma\right] \text{for } r\Sigma_a < 0.1,$$

where r is the sample radius, Σ_a is the macroscopic absorption cross section, and $\gamma = 0.577216\ldots\ldots$ is Euler's constant.

$$\langle P_o \rangle = \frac{\int_{E_o}^{E_m} P_o(E) \frac{dE}{E}^{3/2}}{\int_{E_o}^{E_m} \frac{dE}{E}^{3/2}}$$

where E_m is taken as infinity, and E_o is taken as 2.014, which is the effective cadmium cut-off defined so that the 1/v absorption above E_o in a 1/E flux is equal to the importance weighted integral of the 1/v absorption in the actual spectrum over all energies.

Then,

$$\langle P_o \rangle = 1 - \frac{4}{3} \int_{E_o}^{\infty} r\Sigma_a(E) \frac{dE}{E}^{3/2}$$

$$- 1/2 \int_{E_o}^{\infty} \left[r\Sigma_a(E)\right]^2 \left[\log \left(\frac{2}{r\Sigma_a(E)}\right) + 0.67278\right] - \frac{dE}{E}^{3/2}$$

$$2/\sqrt{E_o}$$

Now,

$$\Sigma_a(E) = \frac{\Sigma_a(E_o)\sqrt{E_o}}{\sqrt{E}},$$

and the energy dependence of

$$\log\left(\frac{2}{r\Sigma_a(E)}\right)$$

may be ignored since it is slowly varying and the term in which it is involved makes only a small contribution.

Therefore,

$$\langle P_o \rangle \approx 1 - \frac{2}{3} r\Sigma_a(E_o) E_o \int_{E_o}^{\infty} \frac{dE^2}{E^2}$$

$$+ 1/4 \left[r\Sigma_a(E_o)\right]^2 E_o^{3/2} \int_{E_o}^{\infty} \left[\log \frac{2}{r\Sigma_a(E_o)}\right.$$

$$\left. + 0.67278\right] \frac{dE}{E}^{5/2}$$

$$\approx 1 - \frac{2}{3} r\Sigma_a(E_o)$$

$$+ \frac{1}{6}\left[r\Sigma_a(E_o)\right]^2 \left[\log\left(\frac{2}{r\Sigma_a(E_o)}\right) + 0.67278\right] .$$

* Case, K. M., deHoffman, F., and Placzek, G., Introduction to the Theory of Neutron Diffusion I, 1953.

APPENDIX D

REACTIVITY EFFECT OF A SCATTERING SAMPLE INSIDE OF THE CADMIUM TUBE

Inside of the cadmium tube the flux is given by the function $\phi(u)$ and the importance of a neutron of lethargy u is given by the function $P(u)$. The shapes of each of these functions are given by multigroup, multizone calculations, and are shown in Figs. 3-1 and 3-2.

The effect of a scattering collision is to remove a neutron of lethargy u and to produce a neutron of lethargy $u + \Delta u$. The reactivity effect of each scattering is proportional to the number of collisions and to the change in importance. We have therefore,

$$\rho_s = C\,NV \int_0^{\infty} \int_0^{\zeta_{max}} \sigma_s(u)\,\phi(u)\,p(\zeta)\,[\,P(u+\zeta)-P(u)\,]\,du\,d\zeta$$

where $p(\zeta)$ is the probability that a scattering event will produce a lethargy change ζ. For small ζ_{max} the change in importance is small and there is a small net positive reactivity effect due to scattering out of the fission spectrum hump in $\phi_1(u)$. For large ζ_{max} a relatively large fraction of the collisions degrade the neutrons into the region of very low importance near the cadmium cutoff and the net reactivity effect is negative. These considerations explain the difference in sign, for instance, in the reactivity coefficients of bismuth and oxygen.

APPENDIX E

A MEHTOD FOR ESTIMATING THE UNRESOLVED RESONANCE INTEGRAL

In the symmetric approximation the resonance capture integral is given by,

$$I_{sym} = 4.08 \times 10^6 \frac{\Gamma_\gamma \Gamma_n}{\Gamma E_o^2}$$

with $\Gamma_n = \Gamma_n^o \sqrt{E_o}$

$\Gamma = \Gamma_\gamma + \Gamma_n^o \sqrt{E_o}$

where Γ_γ and Γ_n^o are constants

$\frac{\Gamma_n}{\Gamma} \longrightarrow 1$ for large values of E_o

therefore

$$I_{sym} = 4.08\ 10^6 \frac{\Gamma_\gamma}{E_o^2}$$

Assuming that the high energy resonances are equally spaced, with spacing δ

$$\sum I_{sym} = 4.08\ 10^6\ \Gamma_\gamma \sum_{n=o}^{n=\infty} \frac{1}{(E+n\delta)^2}$$

where E is the energy of the first unresolved resonance. To obtain the sum,

$$S = \sum_{n=o}^{n=\infty} \frac{1}{(E+\delta n)^2}$$

the function $y = \frac{1}{(E+\delta x)^2}$ is noted to be a monotonically decreasing function

of x, with concavity as shown in the figure below.

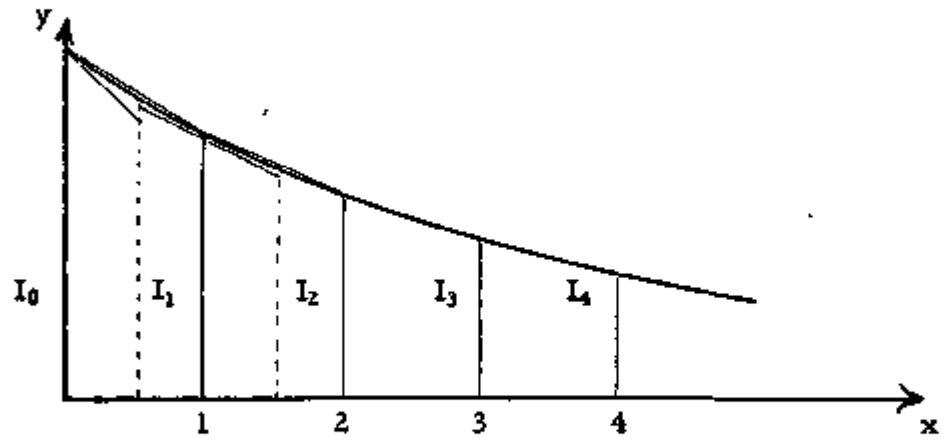

Therefore

$$\frac{I_0 + I_1}{2} + \frac{I_1 + I_2}{2} + \ldots . > \int_0^\infty \frac{\delta x}{(E+\delta x)^2} > I_1 + I_2 + \ldots . + \left(\frac{I_0}{2} - \frac{\delta}{4E^3}\right)$$

but

$$\int_0^\infty \frac{\delta x}{(E+\delta)^2} = \frac{1}{E\delta}$$

Therefore

$$\frac{1}{E\delta} + \frac{1}{2E^2} + \frac{\delta}{4E^3} > S > \frac{1}{E\delta} + \frac{1}{2E^2}$$

For thorium the numerical results are,

E = 1000 ev

δ = 20 ev

Γ_γ = 0.024 ev

S = 5.05×10^{-5}

$\sum I_{sym}$ = 4.945 barns

If this result is multiplied by a correction factor of 0.75 to account for the fluctuations in Γ_n^o a value of 3.71 barns is obtained for the unresolved resonance integral of thorium.

The preceding calculation was based on $\frac{\Gamma_n}{\Gamma} \rightarrow 1$ for large values of E. However, numerical values of Γ_γ and Γ_n^o for thorium are such that this simplification gives an overestimate of the result. An improved estimate may be obtained by retaining the more exact expression,

$$\sum I_{sym} = 4.08 \times 10^6 \, \Gamma_\gamma \sum_n \frac{\Gamma_n^o \sqrt{E_o + n\delta}}{\Gamma_\gamma + \Gamma_n^o \sqrt{E_o + n\delta}} \frac{1}{(E_o + n\delta)^2}$$

for $n \leq 1000$ and reverting to the preceding treatment for $n > 1000$. The result in this case, after correction for the fluctuations in Γ_n^o, is 2.60 barns for the unresolved s-wave resonance contribution.

REFERENCES

1 Pettus, W. G., Samuel, C., and Baldwin, M. N., Report BAW-1244, (1962).

2 Toppel, B. J., Nuc. Sci. and Eng. 5, 88 (1959).

3 Weitman, J., Report AE-99, A. B. Atomenergi, Sweden (1962).

4 Brose, M., Thesis, Technische Hockschule Karlsruhe (1962).

5 Tiren, L. I., and Jenkins, J. M., Report AEEW-R 63, (1962).

6 Nordheim, L. W., Report GA-2563, (1961).

7 Conde, H. and Starfelt, N., Report BNL-694 (N-5), (1961).

8 Maklin, R. L., and Pomerance, H. S., J. Nucl. Energy 2, 243 (1956).

9 Tattersall, R. B., et al, J. Nuc. Energy Part A, 12, 32 (1959).

10 Pettus, W. G., Report BAW-TM-203, (1959).

11 Moore, P. F. G., et al, Report EEW-R57, (1961).

12 Rothman, A. B., and Ward, C. E. W., Nuc. Sci. and Eng. 1, 293 (1962)

13 Thie, J. A., "Heavy Water Exponential Experiments Using ThO_2 and UO_2", Pergamon Press (1961).

14 Dancoff, S. M., and Ginsburg, M., Report CP-2157, (1944)

15 Templin, L. S., Ed., Reactor Physics Constants, ANL-5800, Second Edition, (1963).

DISTRIBUTION

1. U. S. Atomic Energy Commission
Contracts Division
New York Operations Office

M. Plisner (27)

2. U. S. Atomic Energy Commission
Office of Foreign Activities, DRD
Washington 25, D. C.

Dr. R. Carson Dalzell (5)

3. U. S. Atomic Energy Commission
Office of Technical Information
P. O. Box 62
Oak Ridge, Tennessee (3)

4. U. S. Atomic Energy Commission
Reports & Statistics Branch, DRD
Washington 25, D. C.

5. U. S. Atomic Energy Commission
Office of Assistant General Council for Patents
Washington 25, D. C.

Dr. Holton

6. The Babcock & Wilcox Company

Baldwin, MN
Ball, RM
Barringer, HS
Breazeale, WM
CEL Files (2)
Central Files (10)
Craven, JP/ Barberton Library
Deuster, RW (2)
Edlund, MC
Engelder, TC
Lewis, RH
Library, AED (2)
Littrell, LW (2)
Markert, W/Alliance Library
Meem, SH (3)
Pettus, WG (15)
Roberts, DM
Roy, DH
Samuel, C
Snidow, NL
Travis, CC/ TRG
Williams, DVP
Williams, JT
Wittkopf, WA